DOE/NASA/16310-10
NASA TM-102122

The Interface in Tungsten Fiber Reinforced Niobium Metal-Matrix Composites

Toni L. Grobstein
National Aeronautics and Space Administration
Lewis Research Center
Cleveland, Ohio 44135

September 1989

Work performed for
U.S. DEPARTMENT OF ENERGY
Nuclear Energy
Reactor Systems Development and Technology
Washington, D.C. 20545
Under Interagency Agreement DE-AI03-86SF16310

TABLE OF CONTENTS

		Page
I.	**INTRODUCTION**	1
II.	**BACKGROUND**	3
	A. Fiber Reinforcement	3
	B. Diffusion	7
	C. Creep	10
III.	**MATERIALS**	16
	A. Tungsten Fibers	16
	B. Matrix Materials	19
IV.	**PROCEDURES**	21
	A. Fabrication	21
	B. Sample Preparation	25
	C. Creep Testing	27
	D. Sample Analysis	27
V.	**RESULTS AND DISCUSSION**	30
	A. Composite Creep Properties	31
	B. Creep Curves	32
	C. Multiple Linear Regression	37
	D. Interdiffusion Between Fiber and Matrix	41
	E. Effect of Matrix Alloy Additions	53

F. Kirkendall Void Formation 56

G. Effect of Fiber Orientation 59

VI. **CONCLUSIONS** 60

A. Fiber Reinforcement 60

B. Fiber Orientation 60

C. Matrix Alloying Additions 61

D. Comparison to Monolithic Niobium Alloys 61

E. Future Applications 63

VII. **REFERENCES** 64

VIII. **APPENDICES** 68

A. Multiple Linear Regression 68

B. Volume Fraction Determination 70

C. Rule of Mixtures Calculation 73

D. Extrapolation of Fiber Stress-Rupture Data 75

INTRODUCTION

Advanced materials will play a major role in meeting the stringent weight, size, and performance requirements of future space power systems. The requirements for such a system, which may include a service life of greater than 7 years at a temperature in excess of 1350 K, in addition to resistance to liquid metal corrosion, dictate the use of refractory metals. The niobium--1% zirconium (Nb-1Zr) alloy has been suggested for use in such space power conversion applications, but does not have sufficient creep strength for the current design times and temperatures. Further, while current designs of space nuclear power systems specify niobium - base alloys for reactor, heat pipe, and power conversion components, future applications will need materials with greater high-temperature strength and increased creep resistance to meet mission requirements (Titran 1988).

The goal of this research was to improve the creep strength/density ratio of the Nb-1Zr alloy without sacrificing desirable physical properties such as corrosion resistance to liquid alkali metals and low thermal neutron cross section. Fiber reinforcement has been shown to be an effective strengthening method (McDanels et al, 1960), and does not require large alloying

additions to the matrix. Therefore, the feasibility of using metal-matrix composites to meet the anticipated increased temperature and creep resistance requirements imposed by advanced space power systems is of interest. The tensile properties of tungsten fiber reinforced niobium (W/Nb) metal-matrix composites have been explored by Trefilov et al. (1976) and Westfall et al. (1986), and preliminary creep-rupture results were reported by Petrasek and Titran (1988). These studies demonstrated significant improvements in the high-temperature strength/density ratio and the possibility for corresponding mass reductions in high-temperature space power systems.

The intent of this study was to measure the creep properties of tungsten fiber reinforced niobium metal-matrix composites and to evaluate the effect of the fiber/matrix reaction on these properties. Two factors which may affect the fiber/matrix interface, and therefore, the creep properties also were evaluated; small additions of tungsten and zirconium to the niobium matrix, and variation of the orientation of the tungsten fibers relative to the principal stress axis.

BACKGROUND

Fiber Reinforcement

In a typical metal-matrix composite, the fibers reinforce and strengthen an otherwise weak matrix, while the matrix coats and protects brittle fibers which would otherwise fail due to environmental effects. Although it appears to be much simpler to coat a part made from the fiber material than to put fibers into a composite, fiber reinforcement is preferred over coating for two reasons. First, if even a small defect occurs in a coating, the entire core is exposed to the environment. In a fiber-reinforced composite, however, a defect in the matrix exposes only a few fibers, and when they fail, the load is distributed over the remainder of the fibers, making the composite tough. Another reason fiber reinforcement is preferred versus coating is the increase in strength of fibrous over bulk materials.

A composite differs from a monolithic material in that its physical and mechanical properties are defined as that of a structure rather than as a homogeneous or even a heterogeneous material. A composite does not have a characteristic modulus, tensile strength, or even density like a monolithic material does. These values depend on the volume fraction and distribution of

fibers. In a metal matrix composite with a strong interface bond, the tensile and creep strength of the composite depends on the properties of the matrix, the fibers, and the load transfer between the two.

This load transfer results in a very complex stress state. Factors such as residual stresses, multiaxial stresses, and thermally-induced stresses will impact the behavior of the composite. The thermal stresses are due to thermal expansion mismatch between the fiber and matrix. At 1500 K, the coefficient of linear thermal expansion for niobium is 8.75 $x10^{-6}$ K, approximately 40% higher than that for tungsten, 5.15 $x10^{-6}$. This means the matrix wants to elongate both axially and radially, although it is constrained by the stronger fibers. In addition, the composite structure itself can introduce additional sources for crack initiation or different crack paths, and can weaken conventional crack paths. All of these effects are somewhat minimized in this application since little or no thermal or mechanical cycling is involved, but they are not insignificant.

Maximum strengthening in a continuous fiber reinforced composite is achieved by orienting all of the fibers in the composite in a single direction, and then orienting the composite so the applied stress is along the fiber axis. However, since any real application will involve a multiaxial stress state, at least some

strength along more than one axis is required. Angle-plying the fibers is an obvious method of boosting the transverse properties of the composite. However, the effect of changing the fiber orientation on the internal stresses in the composite, especially in the interface, must be understood and quantified.

Another important factor is formation of a reaction zone between the fiber and matrix at elevated temperatures. Since the phase diagram for tungsten and niobium is a continuous solid solution (Figure 1), interdiffusion in this system results in a continuous gradient between the composition of the fiber and that of the matrix across the interface. Obviously, the fiber/matrix reaction will affect and probably degrade the composite's mechanical properties. We must be able to predict this degradation if this composite material is to be used in real systems. If the degradation is substantial, we must look at ways to stop or slow the interdiffusion.

One way to impede interdiffusion in the composite is to create a diffusion barrier between the fiber and matrix. This technique was investigated by Veltri et al. (1975), who ion-plated thermally stable coatings (such as Al_2O_3, Y_2O_3, and HfO_2) onto tungsten wires. Unfortunately, when incorporated into a composite as coated fibers, small cracks in the coatings occurred due to the differential thermal expansion properties between the matrix, coating, and fiber.

It was discovered that these cracks in the coating allowed very fast diffusion of the matrix throughout the fiber/coating interface, leading to fracture of the fiber.

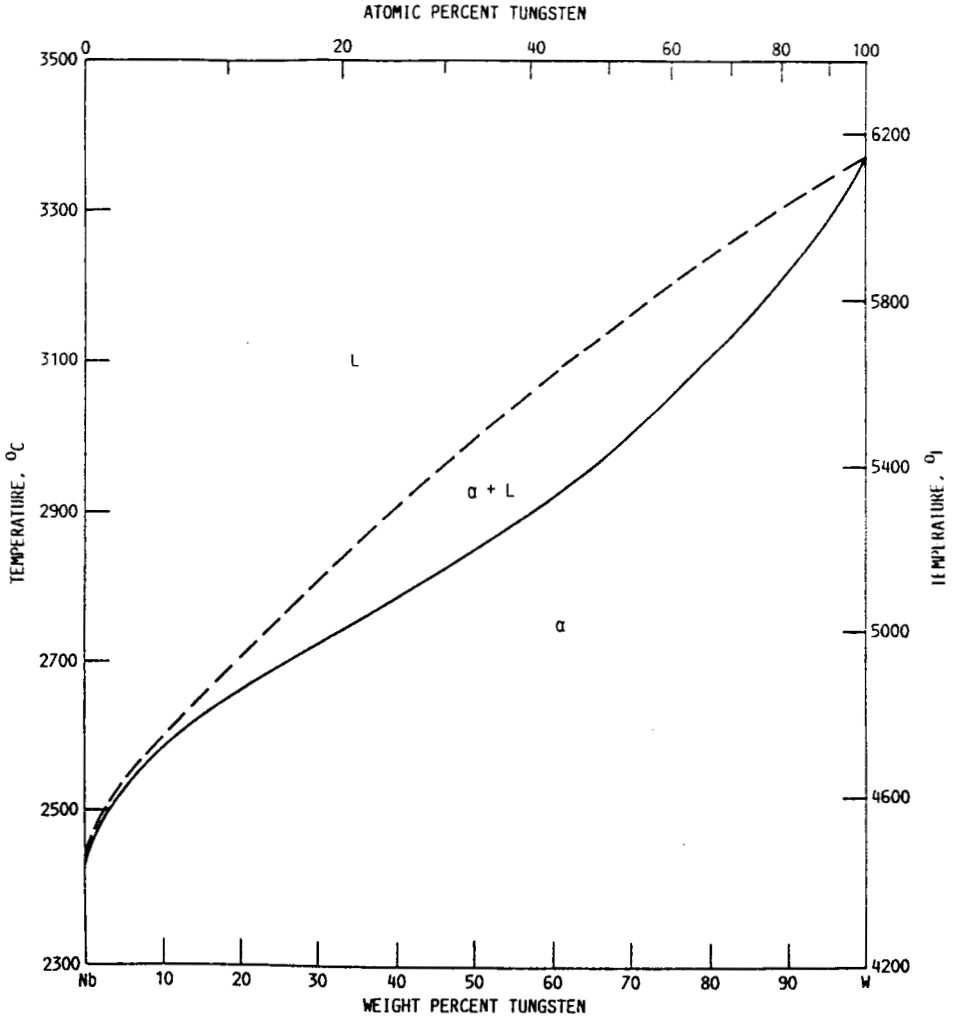

Fig 1 Tungsten - Niobium phase diagram.

The feasibility of ion-implanted diffusion barriers has also been explored. Welsch et al (1987) investigated the concept that a layer of atoms on the fiber surface with considerably larger atomic radii than either the fiber or matrix material may impede interdiffusion. Although this technique shows promise (Kopp et al, 1988), it is far from being applied.

A different method is to make alloying additions to the matrix*. It is known that alloying niobium with tungsten decreases the niobium self-diffusion rate. Several investigation (Lyubimov et al 1967; Lundy and Pawel 1969; Mundy et al 1986; and Hehemann and Leber 1966) have found that increasing the tungsten content in the niobium decreases the diffusion kinetics exponentially across the W/Nb interface. It is possible, therefore, that alloying the matrix material with small amounts of tungsten will decrease interdiffusion rates in the composite. Also, the effect of zirconium in the matrix on the interdiffusion kinetics is of interest, given that Tuchinsky (1979) predicted that alloying niobium with zirconium would decrease its rate of diffusion into tungsten.

Diffusion

Arcella (1974) measured interdiffusion zone growth in the W/Nb system, and found the empirical relationship

*Alloying the fiber is impractical due to the complex chemistry which maintains the high-strength structure of the wire.

Eq 1

$$\ln\left(\frac{\Delta x^2}{t}\right) = -\frac{37390}{T} - 3.869$$

where Δx is the width of the interdiffusion zone in cm, t is the time in seconds, and T is the temperature in Kelvin. He evaluated both arc-cast and CVD tungsten, both with relatively large grain size compared to that in a drawn tungsten fiber.

Arcella found this equation quite accurate over a wide range of times and temperatures. He noted that this was surprising in light of the gross porosity which occurred on the niobium side of the interface in this system. This phenomenon of net mass transport across a diffusion interface, known as the Kirkendall effect, was first observed in the zinc/alpha brass system by Smigelskas and Kirkendall (1947). The Kirkendall effect occurs in a binary solid solution where each of the two atomic species moves with a different velocity. Experimental measurements have shown that the element with the lower melting point diffuses faster (Reed-Hill, 1973); in this case, the niobium. The net mass transfer results in a complex stress state at the interface. The area outside of the fiber which suffers a loss of mass is placed under a two-dimensional tensile stress, while the area just inside the fiber diameter is placed in a state of two-dimensional compressive stess. The stress fields may

bring about plastic flow, with the resulting structural changes normally associated with plastic deformation and high temperatures: formation of substructures, recrystallization, and grain growth.

When the two diffusing species move with greatly different rates during diffusion, voids or pores have been observed in that region of the diffusion zone from which there is a flow of mass. Since every time an atom makes a jump a vacancy moves in the opposite direction, an unequal flow in the two types of atoms just results in an equivalent flow of vacancies in the reverse direction to the net flow of atoms.

The formation of voids, as a result of the vacancy current that accompanies the unequal mass flow in a diffusion couple, is influenced by several factors. It is generally believed that the voids are heterogeneously nucleated on impurity particles. The tensile stress that exists in the region of the specimen where the voids form is also recognized as a contributing factor in the development of voids. If this tensile stress is counteracted by a hydrostatic compressive stress placed on the sample during testing, the voids can be prevented from forming (Barnes and Mazey, 1958).

Arcella found that the void structure, although presenting a reduced cross-sectional area to interdiffusion, did not appear to affect the extrapolation capabilities of his equation. He speculated that perhaps the reduced area for constituent flux was

counteracted by rapid surface diffusion effects within the voids. Also, by the time the pores became gross, the interdiffusion kinetics were considerably reduced.

Hehemann and Leber (1966) measured diffusion coefficients for this system using couples prepared from polycrystalline commercially pure metals. They found that the diffusion coefficients, measured in the temperature range between 1975 and 2575 K, decreased exponentially as the tungsten concentration was increased from 0 to 50 a%, then decreased abruptly at higher concentrations. The diffusion coefficients measured were in the range defined by the self-diffusion coefficients of the individual elements. However, the measured activation energy for interdiffusion was substantially less than that for self-diffusion in the pure components. It was concluded that short-circuit paths, structural irregularities which act as diffusion pipes, developed as a result of the diffusion process itself and contributed significantly to interdiffusion. The relative contributions of volume and short-circuit diffusion appeared to change with temperature and rendered measurements of activation energies and frequency factors meaningless. They also observed Kirkendall porosity at all diffusion temperatures, but found it most severe at the lowest annealing temperature they evaluated, 1975 K.

CREEP

The Rule of Mixtures

It is theoretically possible to predict the properties of a composite based on the properties of the individual components. The simplest method is the two bar model (or the rule of mixtures), given by

Eq 2 $$P_{composite} = \sum P_x \cdot \upsilon_x$$

where P is any physical or mechanical property, such as the elastic modulus or the yield strength, and υ is the volume fraction of each component of the composite. This equation is based on the assumption that the strains in the fiber and the matrix are equal to each other and to that of the composite. If the components, represented by x, include the matrix (m), the fiber (f), and a reaction zone (z) formed between them, the equation is written as,

Eq 3 $$\sigma_c = \sigma_m \upsilon_m + \sigma_f \upsilon_f + \sigma_z \upsilon_z$$

This equation may be expanded to include different fibers or matrix materials in the same composite panel, and other components incorporated into the composite structure, such as cladding materials.

To use this equation, we calculate the volume fraction of each component based on the initial conditions and interdiffusion kinetics. The properties of the fiber and matrix material can be

predicted through tests of each component in isolation, and the properties of the interface region in the W/Nb system can be assumed to be somewhere between the two, since no intermetallic phases form. Therefore, this simple equation can give a rough prediction of composite properties.

The rule of mixtures is most applicable when deformation is elastic and little or no interaction takes place between the components. Creep, however, involves primarily inelastic behavior, and interaction between components is extensive at the temperatures and times of interest. McDanels et al (1967) has shown that the rule of mixtures can be applied to creep of W/Cu composites with certain modifications.

Load transfer is critical in a composite in that the load is applied to the matrix and is effectively carried by the fibers. In a ductile matrix composite with a good interface bond, the load is applied isostatically to the fibers by the surrounding matrix. However, the different properties of the fibers and matrix create a complex stress state during creep deformation. Stresses are induced by the large difference in the yield strengths of the tungsten fiber and the niobium matrix. This means the matrix wants to deform plastically under the applied stress, but is constrained by the fibers which remain elastic at the same stress level.

Creep Mechanisms in Niobium and Tungsten

Gregory and Rowe (1961) have shown that creep of niobium is a diffusion controlled process above 1200 K; and that the addition of 1% zirconium retards polygonization and recrystallization during the 1475 K standard aging treatment and leaves a forest of edge dislocations in the metal. This dislocation forest is stable to about 1375 K, some 170 K above that for pure niobium. Two mechanisms appear to explain this strengthening effect of zirconium; first, ZrO_2 precipitation in dislocations during aging, and second, the diffusion of zirconium atoms to edge dislocations, both of which pin jogs during creep, thus preventing dislocation climb. They also suggest that the presence of interstitial atoms such as oxygen, nitrogen, and carbon on the dislocations increases the binding energy of the zirconium atoms to the jogs. Ye et al (1985) confirms that much of the zirconium exists as a fine zirconia precipitate both within the grains and at the grain boundaries.

Qualitative evidence of grain boundary sliding is quite prominent in creep of niobium, although there is no evidence of void formation and intercrystalline cracking (Begley et al, 1968). At high temperatures, creep deformation is dominated by diffusional creep along grain boundaries and other fast diffusion paths. At low strain rates, the ease with which fold formation at triple points and grain boundary migration occurs seems to preclude stress concen-

trations arising from grain boundary sliding. Hence, creep fracture in niobium is transcrystalline by void formation and coalescence, and the fracture elongation is quite high, 50 to 100% and more.

Pure tungsten exhibits transcrystalline fracture with quite high ductility (Begley et al, 1968). Alloying with dispersed phases, such as thoria, however, promotes intercrystalline fracture which in turn leads to low creep ductility. Disparity in the shear strengths of the internal grain area and the grain boundary would tend to promote intercrystalline cracking if the strains due to grain boundary sliding cannot be relaxed by deformation within the grain. Precipitates might restrain grain boundary migration, and microcracks might form at the grain boundary due to low interfacial adhesion. However, grain boundary precipitates can exert a favorable influence by decreasing the free lengths of grain boundary, which would reduce stress concentrations. Creep failure of doped tungsten wires has been observed to occur by nucleation of voids at potassium-filled bubbles (Briant, 1988).

The Continuum Approach

Much of the previous work in this area has avoided this complex stress analysis and treated the composite as a structure -- the continuum approach. The expected creep life of any material can be predicted using a multiple linear regression model such as Larson-Miller (1952) or Orr-Sherby-Dorn (1954), regardless of its

internal structure. These types of analyses use creep life data measured at several temperatures and applied stress levels to extrapolate predictions for other temperatures and stresses. It is difficult to use this approach with any composite due to varying volume fractions of fiber; although, if known, this can be taken into account. Also, in the case of W/Nb composites, an additional time- and temperature-dependent interface reaction is taking place by interdiffusion between the fiber and matrix which may affect the strength of the composite. If this interdiffusion does affets the strength of the composite and is not take into account, interpretation of the regression analysis is impossible.

MATERIALS

Tungsten Fibers

When tungsten is drawn into a fine wire, the resulting microstructure may have up to five times the strength of the monolithic material (Yih and Wang 1979). The stability of the fibrous grain structure at elevated temperatures is dependent on the grain-boundary pinning mechanism in the wire. The 100-hour creep rupture strengths of three tungsten-based alloy wires are compared to that for unreinforced (monolithic) Nb-1Zr in Figure 2, and micrographs of their longitudinal sections are in Figure 3.

The 218CS tungsten wire is a potassium-doped, commerically available lamp filament. Potassium bubbles pin the grain boundaries, resulting in an increased recrystallization temperature over monolithic (undoped) tungsten (Welsch et al 1979). The ST300 wire is dispersion strengthened with 1.5 w% thoria (~0.1 μm diameter). This wire is slightly stronger than 218CS, due to the increased thermal stability of the thoria dispersoid compared to the potassium bubbles, and is also commerically available. The W-HfC wires are strengthened by a very fine dispersion (0.05 μm diameter) of even more thermally stable hafnium carbide particles, and exhibit superior creep properties. Unfortunately, W-HfC wires were not

available at the time of this study; therefore, only ST300 tungsten fiber reinforced composites were evaluated. The wire had a diameter of 200 μm.

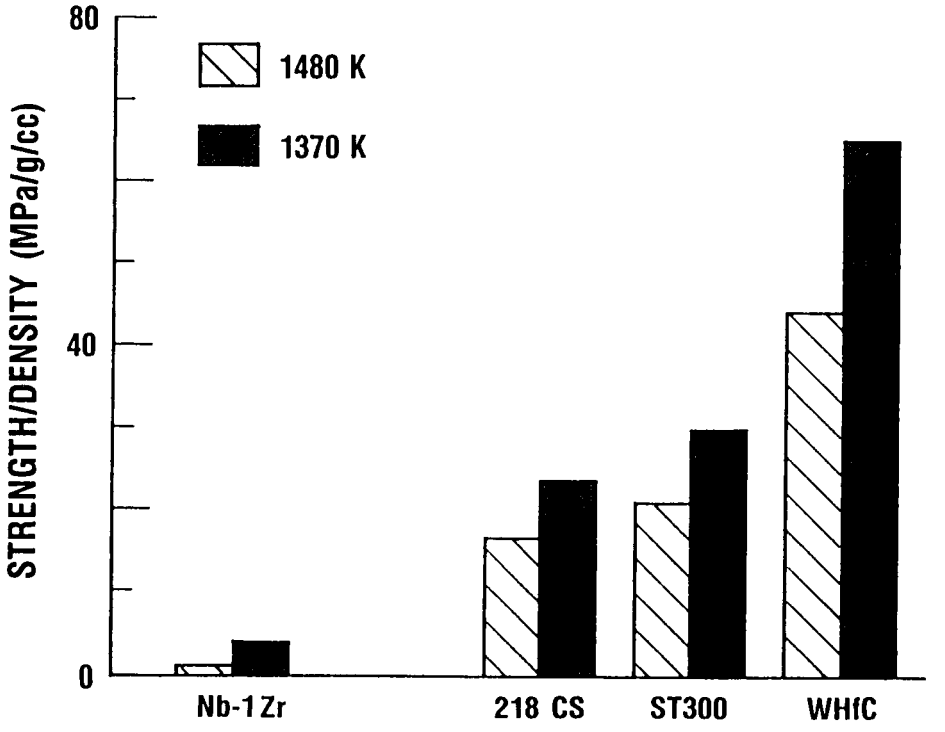

Fig 2 Comparison of the 100-hr creep rupture strength-to-density ratio for three tungsten-based alloy wires versus monolithic Nb-1Zr alloy. (From Tietz and Wilson, 1965; Petrasek, 1972; Petrasek and Beremand, 1987; and Petrasek and Signorelli, 1969.)

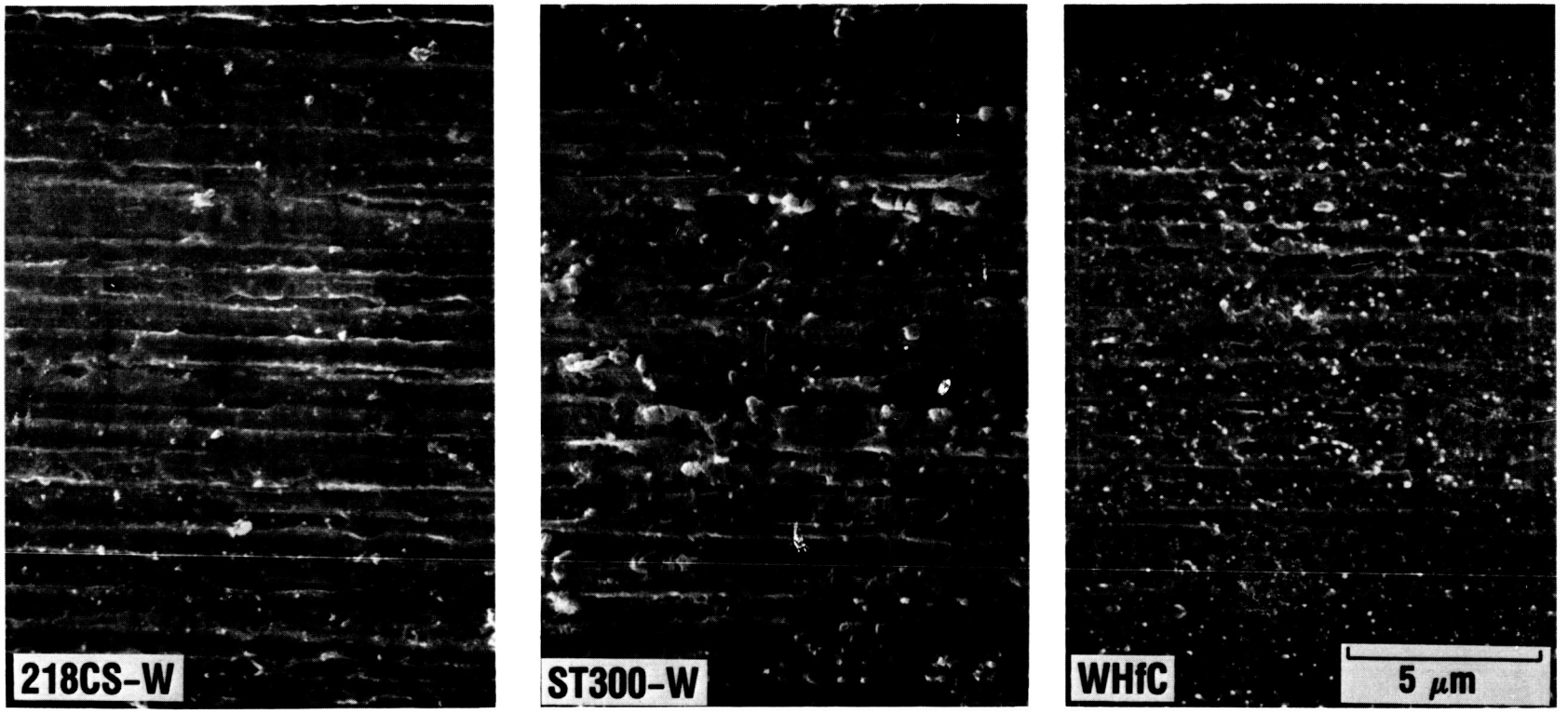

Fig 3 Longitudinal sections of as-drawn tungsten-based alloy wires. The 218-CS wire is a 200 μm fiber doped with potassium; the ST300 wire is also 200 μm diameter with 1.5 w% thoria; the W-HfC has a diameter of 375 μm with ~1 a% hafnium carbide in a fine dispersion.

Matrix Materials

The matrix alloy compositions are listed in Table I. Additions of zirconium (1 and 2 w%) and tungsten (1, 5, and 9 w%) were made to niobium to assess their effect on the fiber/matrix reaction. The small addition of zirconium results in a zirconia precipitate which strengthens the alloy and removes oxygen from the grain boundaries of the niobium*. Tungsten was added to decrease the concentration gradient between the fiber and matrix, and is a solid solution strengthener in niobium.

The matrix materials were obtained in the form of 1.6 mm diameter wire. Specimens of these alloy wires were given a recrystallization anneal and single tensile tests were conducted in vacuum for each composition at 1366 and 1589 K. The strain rate of the tensile tests was .05 m/m. The ultimate tensile strength to density ratios for these alloys are given in Figure 4.

---

*This addition is important to lithium corrosion resistance. Lithia is one of the most stable metal oxides (more stable than zirconia), and if any oxygen is present in the grain boundaries, the liquid metal will leach it out. The lithium can eventually permeate the entire thickness of the container, resulting in "weeping" on the outer wall surface (Hoffman and Harrison, 1968).

Table I. Matrix Alloy Compositions

	w%		a%	
	Zr	W	Zr	W
Nb				
Nb-1Zr	1.1		1.1	
Nb-2Zr-1W	1.8	1.1	1.8	0.6
Nb-1Zr-5W	0.7	4.7	0.7	2.4
Nb-1Zr-9W	1.3	8.8	1.4	4.6

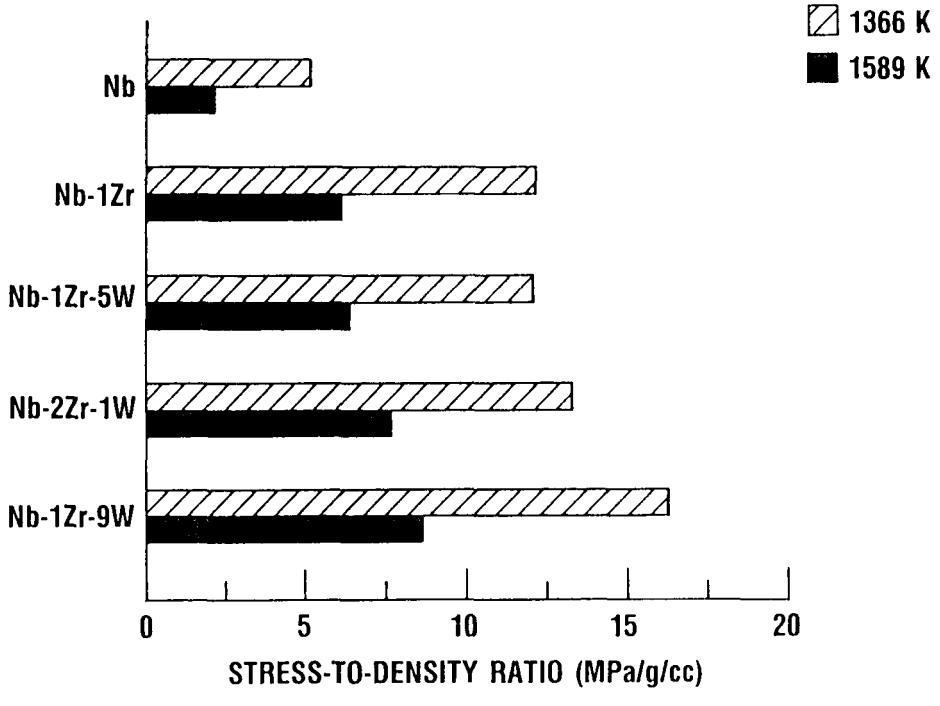

Fig 4 Comparison of matrix alloy ultimate tensile strength-to-density ratios. (compositions in w%)

PROCEDURES

Fabrication

All of the composite panels tested in the program were fabricated using an arc-spray process developed at the NASA Lewis Research Center by Westfall (1985). This process, schematized in Figure 5, consists of wrapping the reinforcing fibers on a drum, placing the drum in an air-tight chamber, evacuating the chamber, and back-filling it with argon. Next, wires of the matrix composition are brought together in the arc-spray gun, an arc is struck between them, and pressurized argon blows the molten matrix material onto the reinforcing fiber mat. The drum rotates until all the fibers are covered; the resulting structure is a "monotape" consisting of one layer of fibers in matrix (Figure 6). Layers of monotapes can then be hot pressed or hot isostatically pressed (HIP), producing a fully densified consolidated structure with negligible fiber/matrix interfacial reaction (Figure 7). Composite panels were fabricated with fibers oriented three ways, as shown in Figure 8. The majority of panels had unidirectionally aligned, axially oriented (0°) fibers. Panels were also fabricated with transversely oriented (90°) fibers, and with angle-plied (±15°) fibers.

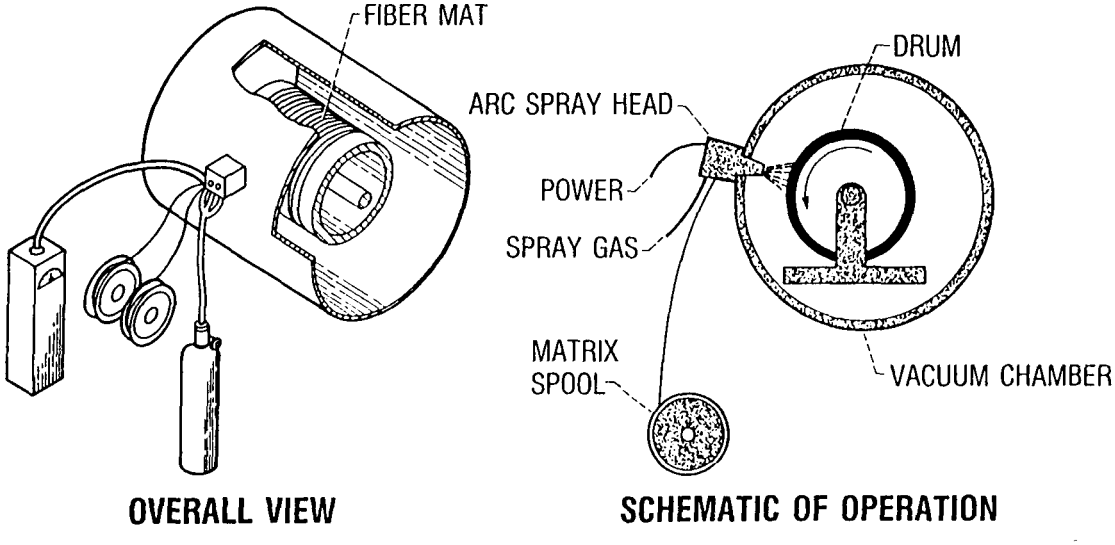

Fig 5 Schematic of the arc-spray fabrication process.

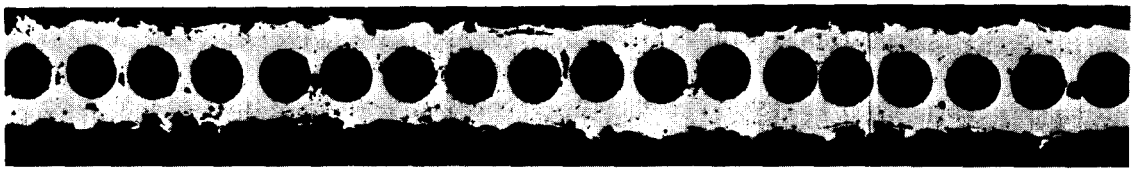

Fig 6 W/Nb as-sprayed monotape.

Fig 7 As-fabricated microstructure of a W/Nb composite containing ~50 v% fiber.

Several factors determine the volume fraction of fiber in the finished composite panel. Most important are initial fiber spacing on the drum and the amount, if any, of cladding used on the panel. Also, the thickness of the sprayed layer, the initial and final density of the sprayed layer, whether or not the monotape was sprayed on both sides will affect the volume fraction of fiber somewhat. The fiber spacing and spraying parameters for this study were specified to produce panels with 40 volume percent fiber, but were not precisely observed. This resulted in a ±25% variation around the 40 volume percent value.

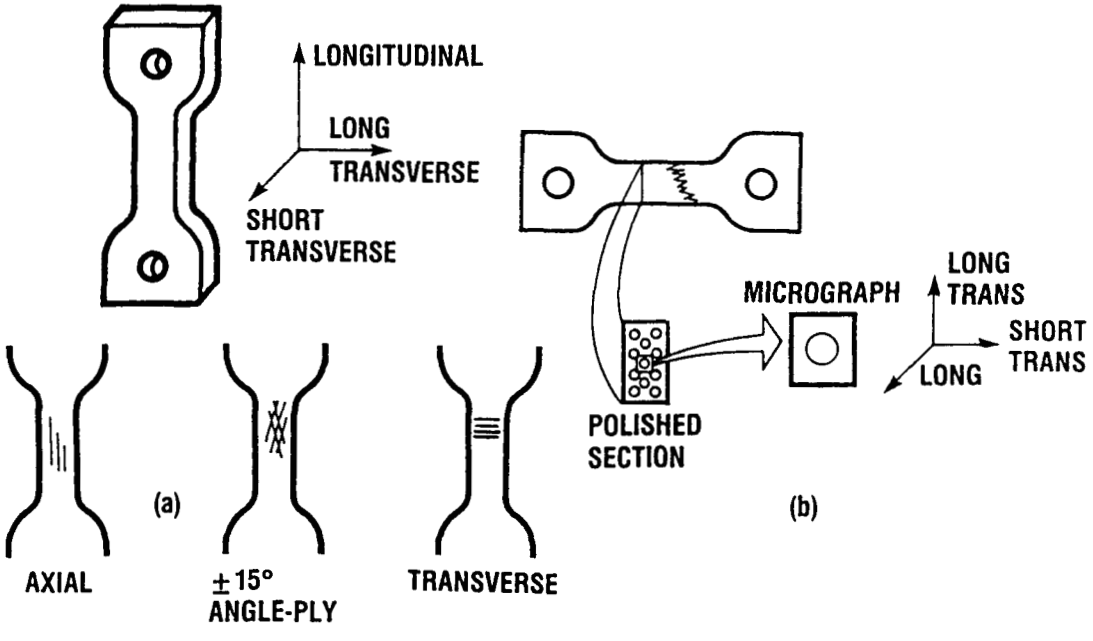

Fig 8 Schematic of the fiber orientations in W/Nb creep specimens.

Additional panels without fibers were fabricated to evaluate the creep strength of the matrix material in the arc-sprayed condition*. Only niobium and Nb-1Zr were tested in this way due to the limited amount of alloy matrix wire material. Unfortunately, the matrix had to be sprayed onto a molybdenum sheet in order to keep it from sticking to the drum (the reinforcing wires normally do this when a monotape is sprayed). The molybdenum sheet had to be etched off of the very porous monotape with nitric acid, thereby increasing the interstitial element contamination of the pressed panel. Consideration of the matrix-only creep data must be influenced by this fact.

Sample Preparation

Creep specimens having a reduced gauge section 25.4 mm long and 6.35 mm wide were electric discharge machined (EDM) from the composite panels. Tungsten or tantalum tabs (0.5 mm thick) were attached to the ends of the samples to prevent shear pullout of the pinhole area. Figure 9 depicts a fractured creep specimen. These tabs were electron beam welded onto the samples with fibers oriented 0° and ±15° to the stress axis; this resulted in several of these samples breaking in the pinhole area during creep testing. Although this was partially ascribed to the fact that alloying niobium with

*Arc-spraying produces a unique matrix microstructure; although it is not "rapidly solidified," it is quickly cooled against the rotating drum, resulting in a fine-grained microstructure.

tungsten embrittles the niobium, the large amount of porosity observed in the weld was more likely at fault. This porosity was ascribed to gases in the arc-sprayed material; either argon bubbles or dissolved oxygen and nitrogen from impurities in the argon. To eliminate this problem, those samples with fibers oriented 90° to the stress axis had tantalum tabs attached to the samples during the HIP cycle.

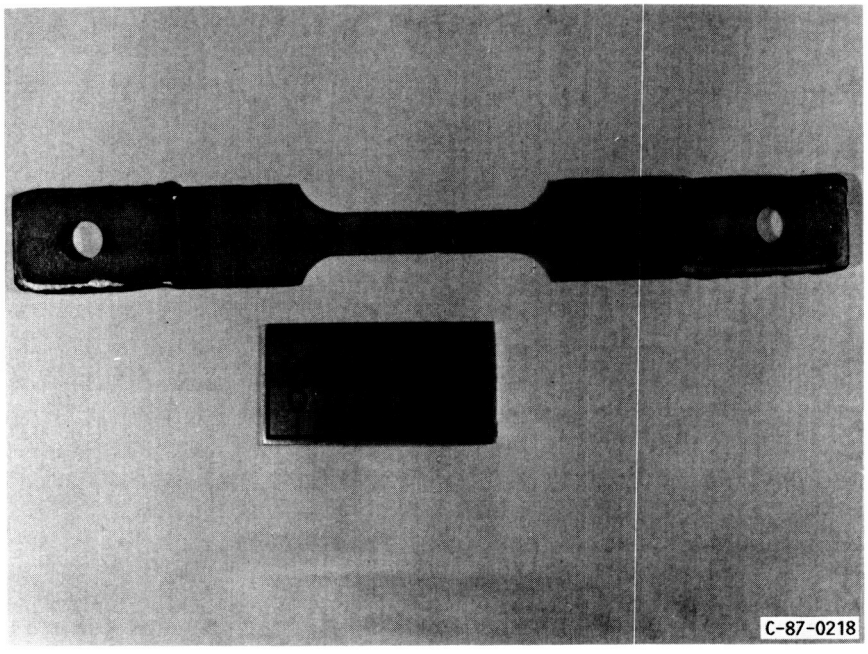

Fig 9 Typical failed W/Nb composites creep specimen. Tungsten tabs (0.5 mm thick) were electron beam welded onto the ends of the samples to prevent shear pullout of the pinhole area.

Creep Testing

Creep-rupture tests in a constant load conditions were conducted in a vacuum of 7×10^{-5} Pa. Creep strains were measured optically via a cathetometer clamped to the furnace chamber frame sighting on Knoop hardness impressions placed 25.4 mm apart in the reduced section. The creep apparatus is fully described elsewhere by Titran and Hall (1965). The precision of creep strain measurements is estimated to be ~0.02% for the gauge length used. The strain on loading was measured and was incorporated in the reported total creep strain.

A limited number of samples were annealed in a vacuum of 10^{-8} Pa without an applied stress to evaluate the effect of temperature without applied stress on diffusion. These pieces were annealed at 1500 and 1800 K for times up to 1000 hr.

Sample Analysis

Specimens were cut from the creep tested samples as shown in Figure 8. Samples were mounted in epoxy and polished using Struers automatic polishing equipment by the procedure in Table II.

Table II. Metallographic Polishing Procedure

	Grinding			Polishing				Finish
Base	SiC	SiC	SiC	SiC	SiC	Diamond	Diamond	SiO_2
Size	320 grit	400 grit	600 grit	10um	5um	3um	1um	.05um
Time	30s	30s	15s+15s	30s	30s	90s	60s	30s
Media	paper	paper	paper	paper	paper	woven cloth	high-nap cloth	chem cloth

These polished samples were examined on an ARL Electron Probe Microanalyzer. Traces were made for niobium and tungsten in selected samples, usually those with longer exposures.

Microhardness measurements on a Buehler Micromet II Microhardness Tester were also made in the unetched condition. Although the lightest weight available was used (10 g), the indentations were too large to determine a gradient of hardness across the interdiffusion zone.

For optical evaluation, the polished specimens were etched for tungsten, then for niobium. The etchants are given in Table III.

Table III. Etching Solutions

Tungsten Etchant (Murakami's)	Niobium etchant
10 g potassium ferrocyanide 10 g potassium hydroxide 100 ml water	30 ml lactic acid 15 ml nitric acid 5 ml hydrofluoric acid
immerse > 15s	swab 15-30s

Individual fibers in the etched samples were photographed using differential interference contrast (DIC) using a Nikon Epiphot-TME Inverted Microscope. Low magnification micrographs (using collimated light) were taken on a Reichert MEF3 Inverted Metallograph. The fracture surfaces were examined in a Cambridge Stereoscan S200 Scanning Electron Microscope.

RESULTS AND DISCUSSION

Composite Creep Properties

Failure Analysis

Typical fracture surfaces of creep-tested specimens are shown in Figure 10. In these micrographs, the matrix appears to have undergone ductile failure, whereas the fibers failed in a brittle manner. In fact, the applied stress on the composite exceeds the elastic limit for the matrix, but the fibers prevent it from failing. It is possible, too, that the matrix may deform plastically without failing, depending on how far the fibers elongate. In that case, the matrix functions primarily as a protective coating for the fibers during creep, but still contributes some strength to the composite. Since conventional failure mechanisms in the matrix are inhibited due to the constraint of the fibers, the matrix withstands a higher applied stress before it deforms plastically than it is able to in a stand-alone test. In addition, substantial grain growth has occurred in the arc-sprayed matrix during exposure at elevated temperatures.

It is assumed that some grain broadening has taken place in the fibers. This grain broadening results in an increased grain width, but does not affect the aspect ratio of the grains, about

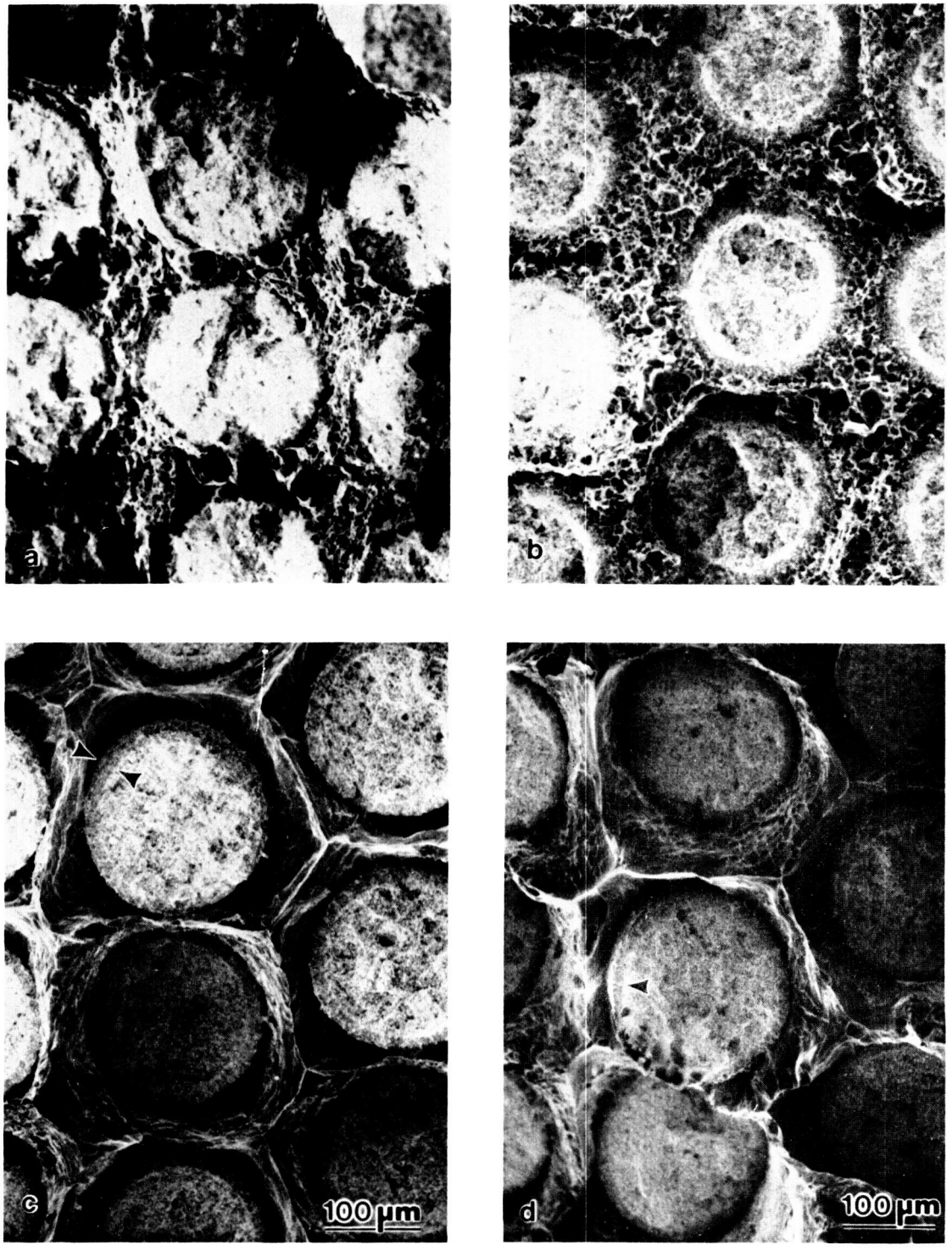

Fig 10 Fracture surfaces of W/Nb composites creep tested at 1500 K under an applied stress of (a) 228 MPa for 425 hr, (b) 80 MPa for 5353 hr, (c) 153 MPa for 937 hr, and (d) 131 MPa for 2485 hr. SEM micrographs reveal the different fracture modes of the fiber and matrix.

200:1. The fibers fail with little apparent necking, although fibers tested singly exhibit substantial necking prior to failure. A reason for that may be that when one fiber reaches the point of necking, it is constrained by the rest of the fibers which have not reached that point, extending the life of the fibers. In fact, Trefilov et al. (1976) found in tensile tests of W/Nb composites that fibers in the matrix achieve 1.5 to 2 time the elongation versus that of the fibers tested separately under the same conditions.

Because the applied stress is divided among all of the fibers, when one or a few fail in creep, the load is redistributed, increasing the load on those remaining. Eventually, the elastic limit of the surviving fibers is reached and they fail transgranularly in tension; this results in a standard 45° failure angle for the axially reinforced composites, with all of the fibers fracturing on about the same plane.

Creep Curves

Since fiber failure dictates composite failure, the creep behavior of the composite resembles that of the tungsten fibers. This behavior is demonstrated in Figure 11, depicting several typical creep curves for W/Nb composite specimens. The curves exhibit primary, steady-state, and tertiary creep.

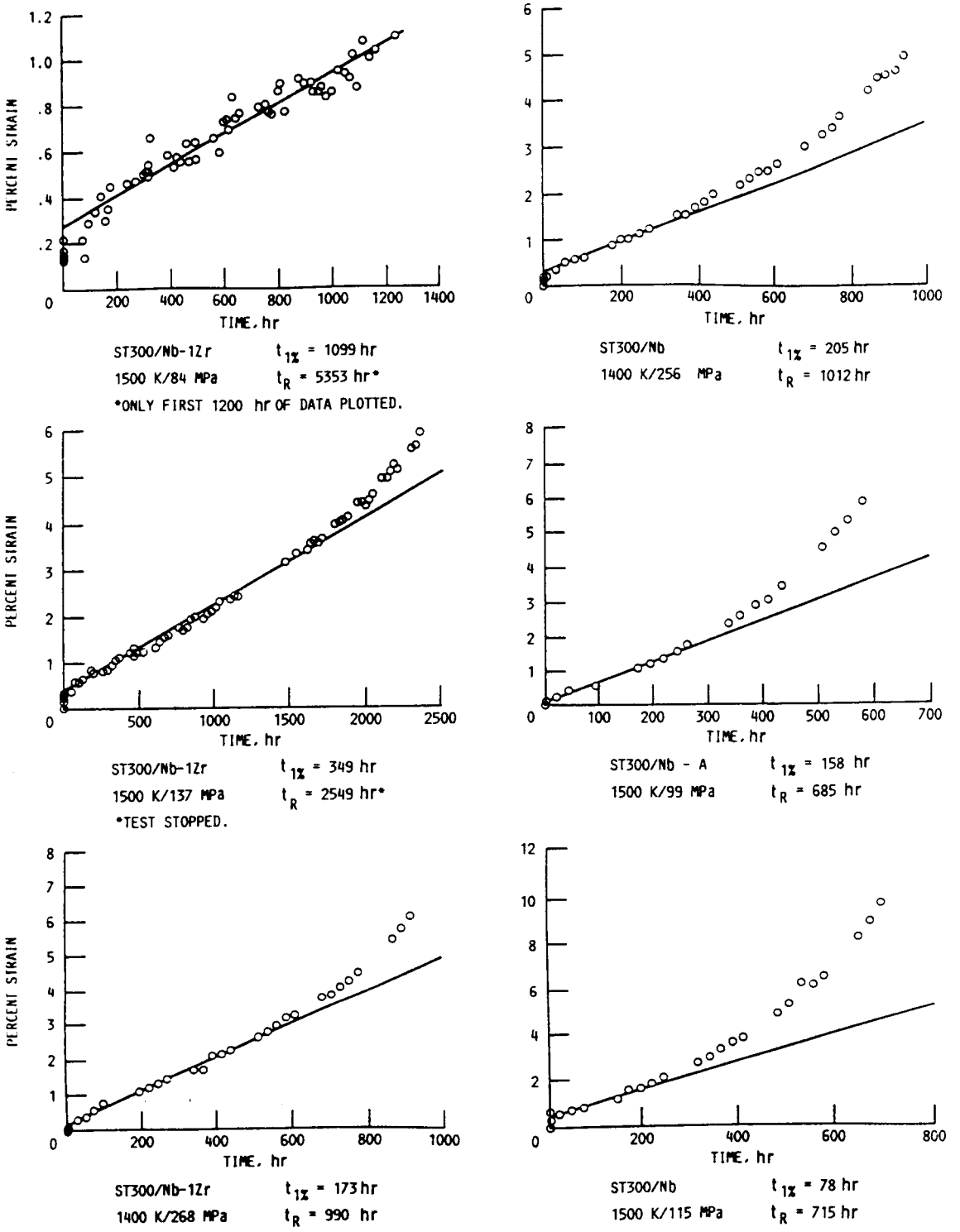

Fig 11 Typical creep curves for W/Nb composites. The curves exhibit primary, steady, and tertiary creep. Lines are fitted to the steady state creep regime.

Three pieces of data were taken from each creep curve: the time-to-rupture, the minimum creep rate (or the slope of the line exhibiting steady state creep), and the time-to-1%-strain, generally a point on that line. The results for the composite samples are given in Table IV. Since the fiber content varied from ~35 to 52 volume percent, applied creep stresses were normalized to 50 volume percent fiber for comparison purposes by the following equation,

Eq 4
$$\frac{\sigma_{app}}{35\,v\%} = \frac{\sigma_{norm}}{50\,v\%}.$$

This equation assume the entire load is carried by the fibers, and is therefore not a true normalization. Although it is valid for comparing axially reinforced composites to other axially reinforced composites, and for comparing angle-plied composites to other angle-plied composites, it may not be valid for comparing composite structures with different fiber orientations to each other. The alternative, however, is to compare the data by the applied stress regardless of volume fraction. The latter approach is definitely not valid, so the creep data for axial and angle-plied composites plotted here has been normalized. Fracture of the transverse samples appears to occur solely in the matrix (Figure 12), so it is more correct to use the actual applied stress in this case.

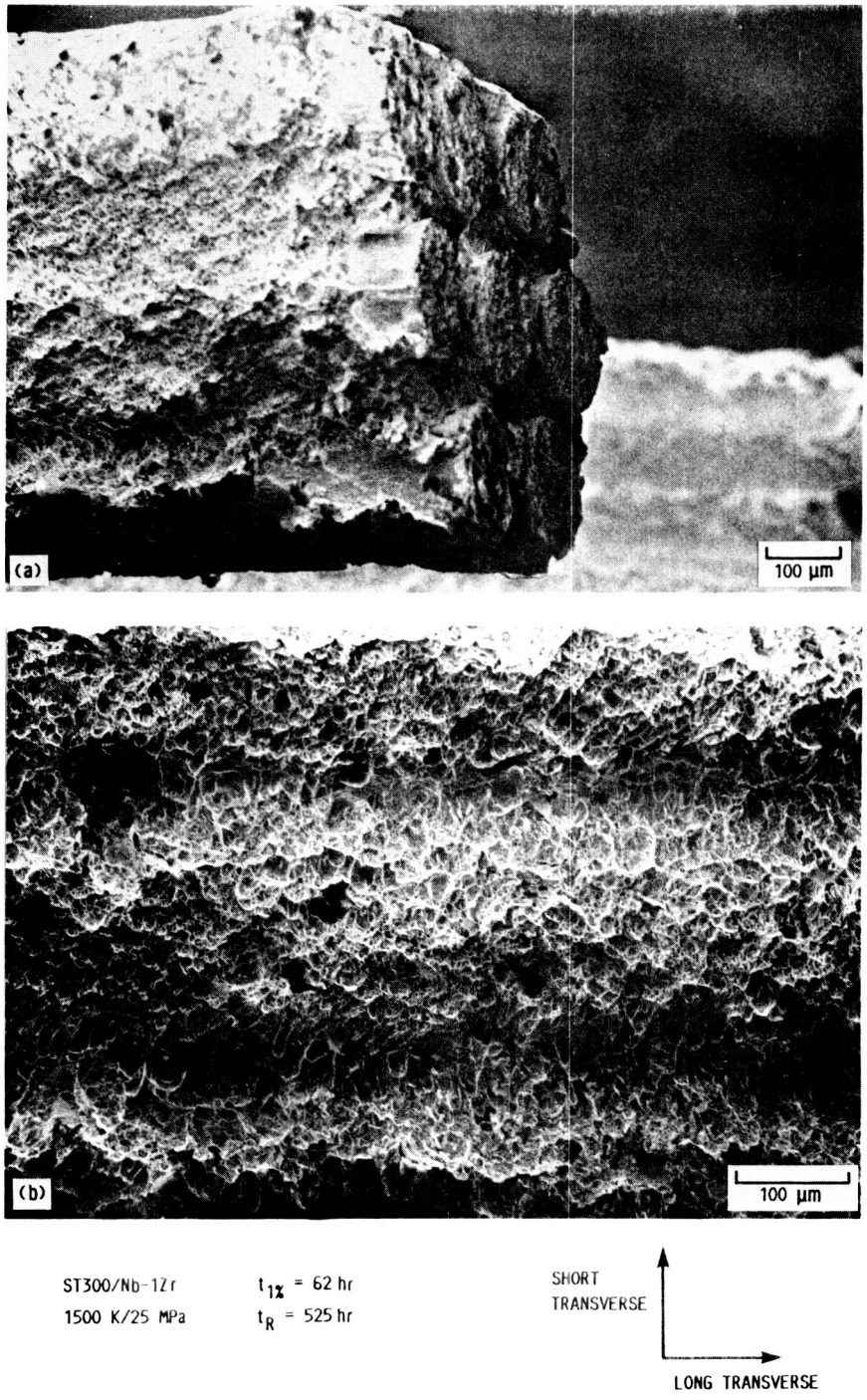

Fig 12 Fracture surfaces of a W/Nb composite with transversely-oriented fibers exhibiting ductile failure in the matrix. At top, a bundle of 7 fibers which has partially debonded from the main part of the composite is depicted. At bottom, the matrix after the fibers have pulled away is shown.

Table IV. Composite Creep Data

Specimen	Temp (K)	Applied Stress (MPa)	Normalized Stress (MPa)	time-to-1% strain (h)	time-to-rupture (h)	volume percent of fiber	minimum creep rate(s^{-1})
ST300/A1*	1400	180	239	243	1894	38	7.28×10^{-9}
ST300/A1	1400	190	255	29	426	37	3.10×10^{-8}
ST300/A1	1400	200	266	16	266	38	3.47×10^{-8}
ST300/A1	1400	250	335	10		37	2.39×10^{-7}
ST300/A1	1500	130	169	17	282	38	3.81×10^{-8}
ST300/A1	1500	150	198	23		38	7.63×10^{-8}
ST300/A1	1500	160	211	16	73	38	1.52×10^{-7}
ST300/A1	1500	200	265	7	20	39	5.50×10^{-7}
ST300/A1	1500	220	295	3	9	37	8.74×10^{-7}
ST300/A5*	1400	200	250	128	683	40	1.71×10^{-8}
ST300/A5	1500	130	171	79	601	38	2.27×10^{-8}
ST300/A5	1500	150	193	40	227	39	5.32×10^{-8}
ST300/A9*	1400	190	248	108	585	38	1.85×10^{-8}
ST300/A9	1400	200	265	68	521	38	1.80×10^{-8}
ST300/A9	1500	130	173	91	552	38	2.77×10^{-8}
ST300/A9	1500	150	202	65	351	37	3.74×10^{-8}
ST300/Nb	1400	160	256	205	1012	31	8.74×10^{-9}
ST300/Nb	1400	180	295	78	315	31	2.51×10^{-8}
ST300/Nb	1400	180	238	243		38	7.80×10^{-9}
ST300/Nb	1400	190	264	233	850	36	9.70×10^{-9}
ST300/Nb	1400	200	270	102		37	1.90×10^{-8}
ST300/Nb	1400	200	327	32	161	31	5.62×10^{-8}
ST300/Nb	1400	210	288	56	387	37	2.95×10^{-8}
ST300/Nb	1400	220	303	40	249	36	3.12×10^{-8}
ST300/Nb	1500	80	110	705	3548	36	6.24×10^{-8}
ST300/Nb	1500	95	128	825		37	2.93×10^{-9}
ST300/Nb	1500	100	131	710	2485	38	3.20×10^{-9}
ST300/Nb	1500	110	153	178	937	36	1.04×10^{-8}
ST300/Nb	1500	120	203	93	475	30	2.12×10^{-8}
ST300/Nb	1500	130	200	95	426	32	3.51×10^{-8}
ST300/Nb	1500	130	180	88	344	26	2.20×10^{-8}
ST300/Nb	1500	150	191	56	284	39	3.15×10^{-8}
ST300/Nb-A*	1400	140	235	93	372	30	2.59×10^{-8}
ST300/Nb-A	1400	150	247		245	30	7.55×10^{-8}
ST300/Nb-A	1400	150	210	180	972	36	1.35×10^{-8}
ST300/Nb-A	1400	160	266	21	90	30	1.07×10^{-7}
ST300/Nb-A	1400	180	258	54	369	35	4.23×10^{-8}
ST300/Nb-A	1500	65	102	158	685	32	1.62×10^{-8}
ST300/Nb-A	1500	70	119	78	715	29	1.63×10^{-8}
ST300/Nb-A	1500	85	119	126	822	36	1.88×10^{-8}
ST300/Nb-A	1500	90	131	72	388	34	3.53×10^{-8}
ST300/Nb-A	1500	90	153	24	133	29	1.05×10^{-7}
ST300/Nb-A	1500	110	191	5	44	29	5.49×10^{-7}
ST300/Nb-A	1500	150	255	1	5	29	3.59×10^{-6}
ST300/Nb-1Zr	1400	160	268	173	990	30	1.33×10^{-8}
ST300/Nb-1Zr	1400	180	290	79	457	31	3.68×10^{-8}
ST300/Nb-1Zr	1400	180	216	238	1490	42	7.04×10^{-9}
ST300/Nb-1Zr	1400	200	218	277	1614	46	8.43×10^{-9}
ST300/Nb-1Zr	1400	200	250	240	1104	40	9.26×10^{-9}
ST300/Nb-1Zr	1400	220	217	340	2325	51	6.56×10^{-9}
ST300/Nb-1Zr	1400	250	263	70	379	47	2.64×10^{-8}
ST300/Nb-1Zr	1400	260	417	6	33	31	4.11×10^{-7}
ST300/Nb-1Zr	1500	60	84	1099	5353	36	1.83×10^{-9}
ST300/Nb-1Zr	1500	100	139	119		36	2.14×10^{-8}
ST300/Nb-1Zr	1500	100	137	349		37	5.28×10^{-9}
ST300/Nb-1Zr	1500	110	155	212	999	36	1.18×10^{-8}
ST300/Nb-1Zr	1500	120	145	106	742	41	1.70×10^{-8}
ST300/Nb-1Zr	1500	130	133	190	921	49	9.65×10^{-9}
ST300/Nb-1Zr	1500	160	170	72	425	47	2.77×10^{-8}
ST300/Nb-1Zr	1500	206	217	17	53	47	1.17×10^{-7}
ST300/Nb-1Zr-A	1400	150	254	39		30	4.62×10^{-8}
ST300/Nb-1Zr-A	1400	180	313			29	
ST300/Nb-1Zr-A	1400	190	341	14	197	28	6.70×10^{-8}
ST300/Nb-1Zr-A	1500	70		204			5.52×10^{-9}
ST300/Nb-1Zr-A	1500	80	144	65	944	28	1.92×10^{-8}
ST300/Nb-1Zr-T*	1500	28		42	680	40	5.25×10^{-8}
ST300/Nb-1Zr-T	1500	25		62	525	41	2.62×10^{-8}
ST300/Nb-1Zr-T	1500	20		105	819	41	1.77×10^{-8}

*A1 denotes Alloy matrix Nb-2Zr-1W

*A5 denotes Alloy matrix Nb-1Zr-5W

*A9 denotes Alloy matrix Nb-1Zr-9W

*A denotes angle-plied (±15°) fibers

*T denotes transverse oriented fibers

The time-to-rupture versus the normalized applied stress plotted in Figure 13 compares the composites at 1400 K and 1500 K. and the minimum creep rates taken from the creep curves are compared in Figure 14. Various aspects of these data will be discussed in the following sections.

Multiple Linear Regression

Multiple linear regression of the creep data for the niobium matrix-only samples, ST300 fibers, and ST300/Nb composites was used to generate equations for $\dot{t}_R$, according to the Orr-Sherby-Dorn (1954) analysis, of the form,

Eq 5
$$\dot{t}_R = C \cdot \sigma^n \cdot e^{-\frac{Q}{RT}}$$

where $\dot{t}_R$ is a "pseudo" creep-rupture rate with units of hr^{-1} taken as the slope of the straight line drawn from the origin to the point of failure on a plot of time versus applied stress*. The applied stress in MPa is denoted by σ, raised to n, the stress exponent. The argument of the exponential is (-Q/RT), where Q is the

*Similarly, $\dot{t}_{1\%}$ is the slope of the line drawn from the origin to the point where the sample reached 1% strain. The units are therefore 0.01/hr.

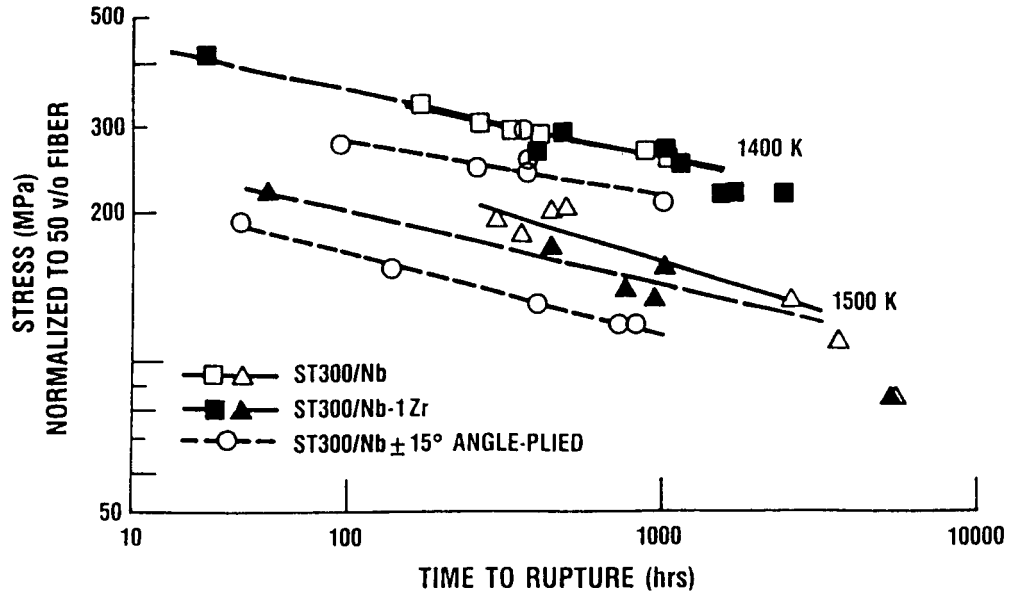

Fig 13 Time-to-rupture vs the normalized applied stress (50 v%) for W/Nb composites creep-tested at 1400 and 1500 K.

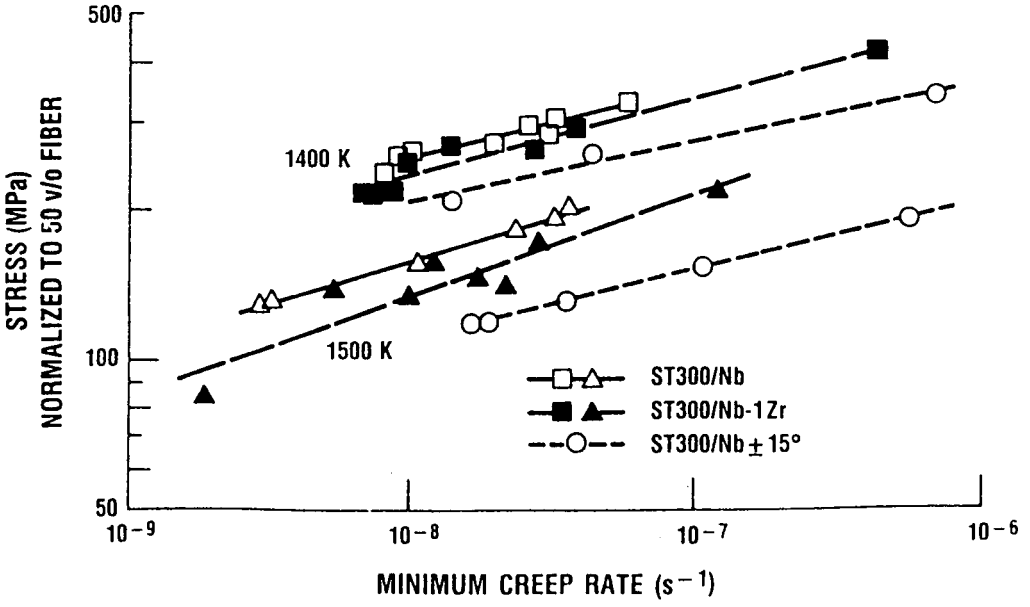

Fig 14 Minimum creep rate vs the normalized applied stress (50 v%) for W/Nb composites creep-tested at 1400 and 1500 K.

activation energy in joules/mole, R is the gas constant (8.3144 joules/degree-mole), and T is the temperature in Kelvin. The computer analysis used to determine the constants in this equation is included in Appendix A.

The following equation was found for the ST300/Nb composites (from data in Table IV),

Eq 8
$$\dot{t}_R = 2.05 \cdot \sigma^{5.11} \cdot e^{-\frac{50000}{T}}$$

The creep data for the niobium matrix-only creep samples is listed in Table V. Regression analysis produced the following,

Eq 6
$$\dot{t}_R = 4.28 \times 10^{18} \cdot \sigma^{4.17} \cdot e^{-\frac{85000}{T}}$$

Table V. Matrix Creep Data

Specimen	Temp (K)	Applied Stress (MPa)	time-to-1% strain (h)	time-to-rupture (h)	minimum creep rate (s^{-1})
Nb	1400	10	347		7.69×10^{-9}
	1400	15	233		1.06×10^{-7}
	1400	18	54	754	5.17×10^{-8}
	1400	20	17	60	1.00×10^{-7}
	1400	20	12	242	1.85×10^{-7}
	1400	25	5	29	5.00×10^{-7}
	1500	5	56	523	3.90×10^{-8}
	1500	10	7	79	3.20×10^{-7}
	1500	10	8	93	2.99×10^{-7}
	1500	15	3	69	7.80×10^{-8}
Nb-1Zr	1400	15	51		1.19×10^{-8}
	1400	20	6	1607	1.20×10^{-7}
	1400	25		728	
	1400	35	1		7.76×10^{-7}
	1500	5	995		1.59×10^{-8}
	1500	10	7		4.16×10^{-7}
	1500	20		892	1.23×10^{-7}

Stress-rupture data for ST300 wire (Petrasek and Titran 1988, Petrasek and Beremand 1987) is listed in Table VI. The creep equation derived from this data was,

Eq 7

$$t_r = 8.42 \times 10^{-12} \cdot \sigma^{6.58} \cdot e^{-\frac{27000}{T}}$$

Table VI. ST300 Fiber Stress-Rupture Data

Temp (K)	Applied Stress (MPa)	time-to-rupture (h)
1255	724	218
1255	724	126
1255	758	192
1255	793	89
1366	483	548
1366	552	85
1366	552	87
1366	621	53
1366	690	22
1366	758	7
1400	414	402
1400	448	333
1400	448	192
1400	4783	99
1400	483	124
1400	483	131
1400	517	64
1400	552	34
1400	586	33
1400	586	23
1400	620	15
1400	620	20
1400	620	15
1400	690	5
1400	690	11
1400	758	3
1478	276	1069
1478	245	172
1478	414	49
1478	483	17
1478	552	6
1478	621	2
1500	280	534
1500	310	343
1500	345	105
1500	245	189
1500	279	32
1500	379	40
1500	414	20
1500	414	34
1500	448	13
1500	483	6
1500	517	3.9

Interdiffusion between Fiber and Matrix

In addition to creep-tested composite specimens, samples were annealed for 100, 500, and 1000 hrs to evaluate interdiffusion in the absence of an applied stress. The width of the interdiffusion zone for both types of specimens was measured by electron probe microanalysis. A sample trace is shown in Figure 15. The results of these microprobe traces are plotted in Figure 16, where they show good correlation to diffusion data found in the literature. We might expect differences due to the different microstructure of the

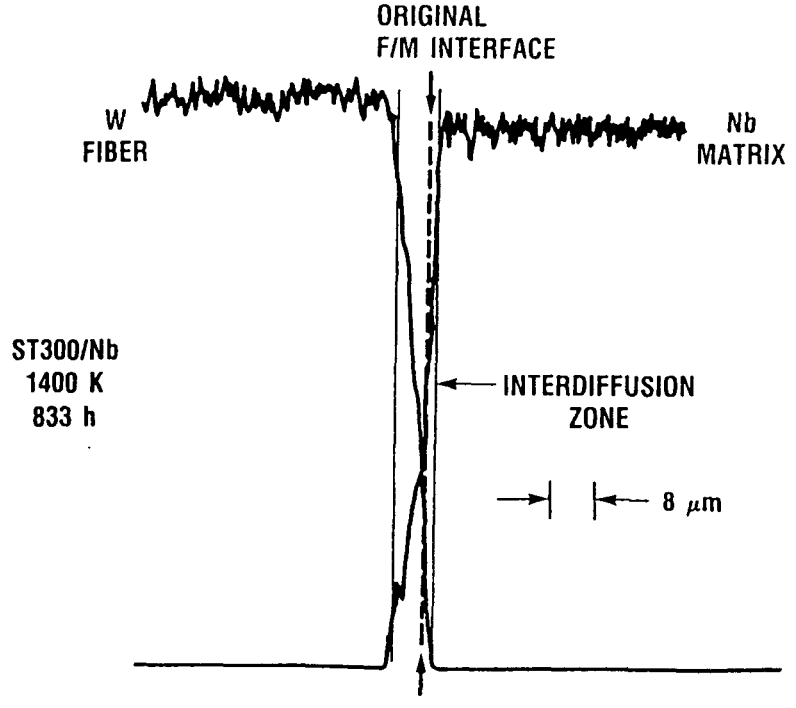

Fig 15 Typical microprobe trace across the fiber/matrix interface in a ST300/Nb composite exposed to 1400 K in vacuum for 833 h under a normalized applied stress of 238 MPa. The extent of interdiffusion is indicated taking the limitations of the instrumentation into account. The position of the original fiber/matrix interface implies that the mjority of the diffusion occurs from the matrix into the fiber.

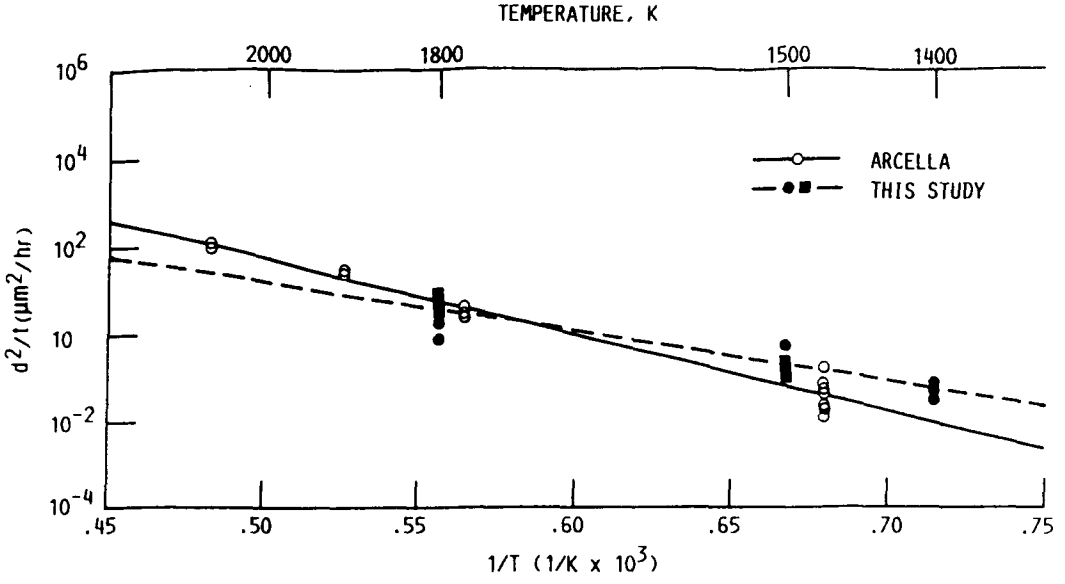

Fig 16 Comparison of diffusion results to Arcella (1974). Circles represent composite specimens with a niobium matrix; squares, a Nb-1Zr matrix.

tungsten used; the arc-cast and CVD tungsten Arcella evaluated is quite different from the fine-grained tungsten in a drawn fiber. It appears, however, that diffusion is controlled by bulk processes at these temperatures (Hehemann and Leber 1966). Also, the radius of curvature of the interface in the composite may influence diffusion coefficients. However, these effects have been found to be minimal with 200 μm fibers (Kopp et al 1988). The measured data fits the equation,

Eq 9

$$\ln\left(\frac{\Delta x^2}{t}\right) = -\frac{26692}{T} + 16.4$$

where Δx is the width of the interdiffusion zone in μm, t is the time in hours, and T is the temperature in Kelvin. This equation relates the extent of the diffusion to the time and temperature of exposure. In addition, a plot of the diffusion at 1400, 1500, 1800 K versus the square root of time is given in Figure 17, which exhibits traditional diffusion behavior according to the $t^{1/2}$ dependence. No difference was observed between Nb and Nb-1Zr matrix composites.

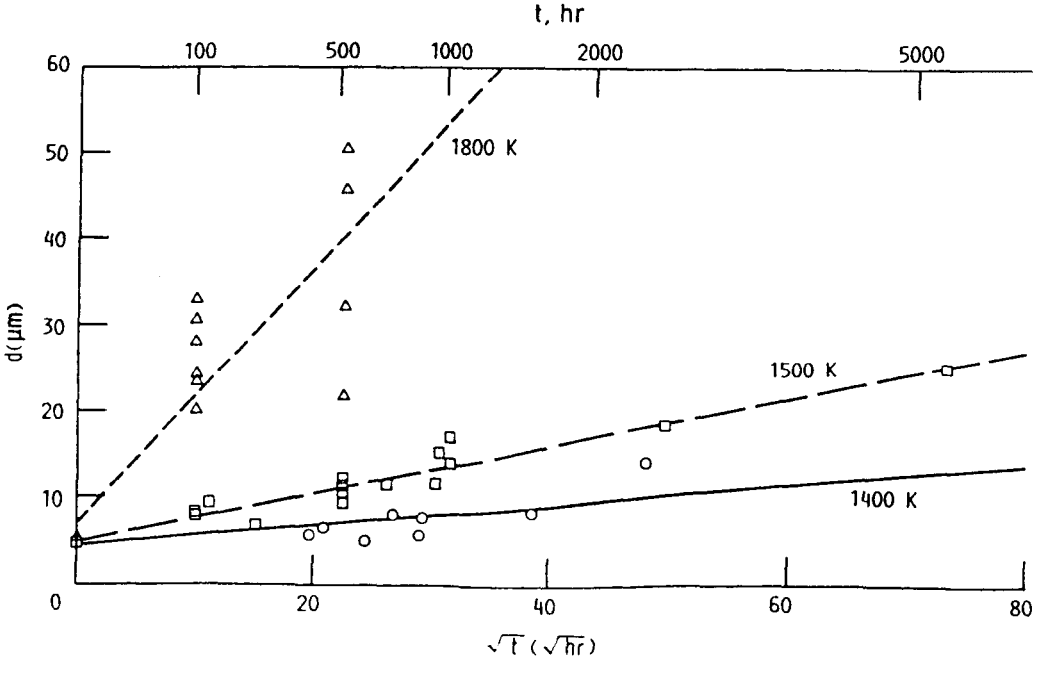

Fig 17 Comparison of the extent of interfacial diffusion at various temperatures.

The interdiffusion between the fiber and matrix which occurs upon elevated temperature exposure is also apparent in the fracture micrographs (Figure 10), where the measured diameter of the fibers including the reacted areas does not appear to have changed from the as-fabricated condition (~200 μm). In fact, microprobe traces of the fiber/matrix interface indicate that the majority of the diffusion is into the fiber (Figure 15). When the polished sections are examined (Figure 18), a recrystallized zone is evident within the original outer diameter of the fiber. These facts show that niobium diffuses into the fiber and lowers its recrystallization temperature, resulting in a recrystallized and tungsten-depleted area within the original fiber diameter.

In Figures 13 and 14, a negative deviation from the established slope of each of the lines is apparent for specimens subjected to relatively low applied stresses. Since these specimens were tested for correspondingly long times in a relatively poor vacuum, the negative deviation may be due to intersitital reaction in the matrix--niobium forms a volatile oxide at these temperatures. However, it may also be attributable to the growth of the fiber/matrix reaction zone. This recrystallized area of the fiber no longer has the high-strength fibrous grain structure, and no longer contributes to the strength of the composite in the capacity it did at the start of the test.

Fig 18 Transverse sections of W/Nb Composites creep-tested at 1500 K under a normalized appled stress of (a) 137 MPa for 2549 hr, and (b) 80 MPa for 5353 hr. Metalographic preparation illustrates the reaction zone between the fiber and matrix.

We can use a simple calculation to assess the effect of the strength of the interface on the strength of the composite. Recall the rule of mixtures,

Eq 3 $$\sigma_c = \sigma_m v_m + \sigma_f v_f + \sigma_z v_z$$

which, as was mentioned previously, does not account for inelastic behavior of the components. However, positive or negative deviation from this equation can help us to understand the composite creep behavior. We can calculate the volume fractions of each of the components by making some assumptions about the interdiffusion and the initial volume fraction. These calculations are detailed in Appendix B.

Eq 10 $$v_m = 0.5$$

Eq 11 $$v_f = \frac{(D_o - 2x)^2}{2D_o^2}$$

Eq 12 $$v_z = 0.5 - \frac{(D_o - 2x)^2}{2D_o^2}$$

Now, Eqn 9 gives an expression for Δx, the width of the reaction zone as a function of time and temperature. Since we also

know the original fiber diameter D_o, we now have expressions for the volume fractions of each component as a function of time and temperature.

We also have expressions for the creep strength of the niobium matrix material (Eqn 6) and the ST300 fiber (Eqn 7). Now, the only unknown in Eqn 3 is the creep strength of the interface zone. In order to better estimate these properties, microhardness measurements were taken on the fiber, matrix, and the interface zone. Figure 19 contains several micrographs displaying the position of the indentations and their corresponding hardness readings. Only a few samples had a reaction zone of sufficient width to accomodate the entire indentation. Because of the composition gradient, an indentation which encompassed the recrystallized zone exactly might best represent the hardness of the interface layer. The measured hardnesses indicate that the reaction zone is somewhere in between the properties of the fiber and the matrix, but actual estimations are impossible due to the placement and limited number of the indentations. Some of the samples exposed for very long times exhibited hardening of the matrix phase; this was ascribed to extensive oxidation of the matrix during testing.

Further, we can calculate the creep strength of the composite using Eqn 3 while varying the properties of the interface zone from

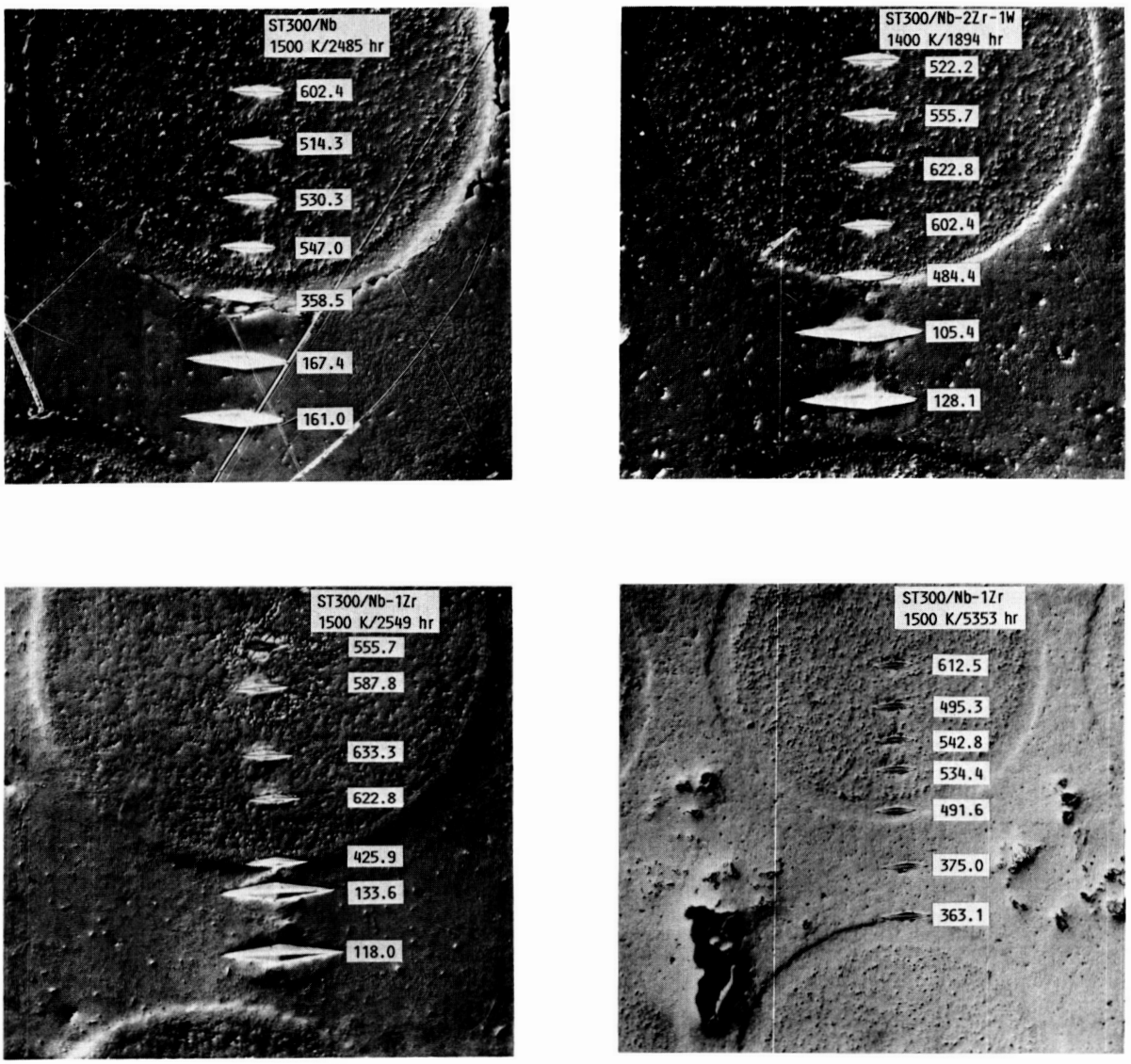

Fig 19 Microhardness measurements of composite sections after creep testing.

that of the fiber to that of the matrix*. Three cases are plotted in Figure 20, where the properties of the interface are set equal to those of the matrix, to those of the fiber, and to an average between the two. It is seen that at higher stresses, where the samples are exposed to temperature for correspondingly shorter times, the difference between the three cases vanishes. Therefore, one can see that at shorter times, the width of the reaction zone is small, so the value for v_z is also small; this minimizes any differences in σ_z. At lower stresses (and longer times), the difference becomes appreciable.

However, when the creep strengths of all the components are plotted together, as in Figure 21, the small differences arising from the strength of the interface zone become secondary. No matter what value is used for interface strength, the measured creep properties exceed those calculated from the rule of mixtures. Therefore, the creep strength of the composite is greater than the combined creep strengths of its components. There may be several reasons for this synergistic effect.

The factors present in the composite that do not exist in stand-alone tests include inelastic strains due to differential thermal expansions and diffusion effects. It is unlikely that

*Calculation detailed in Appendix C.

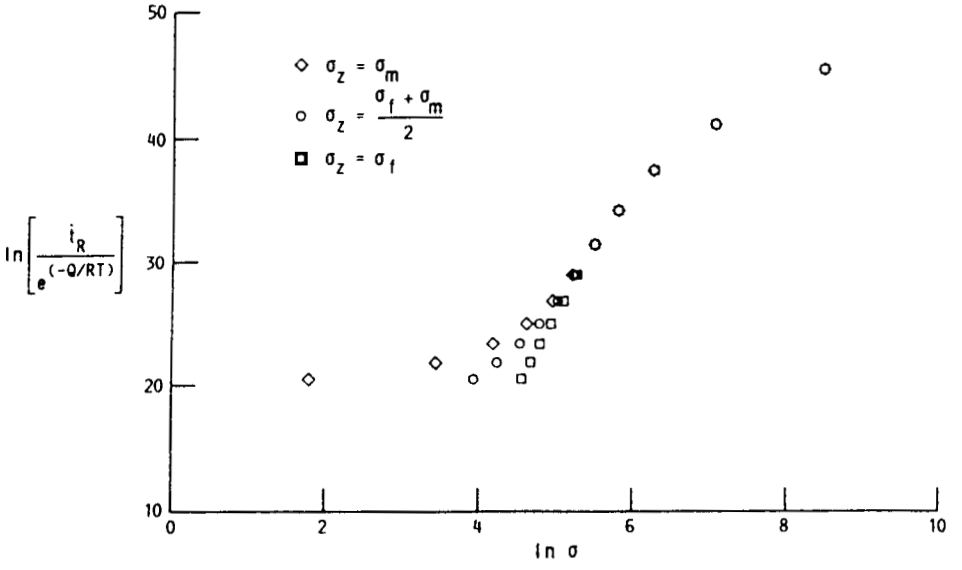

Fig 20 Calculated strength of the composite using Eq 10 varying the properties of the reaction zone.

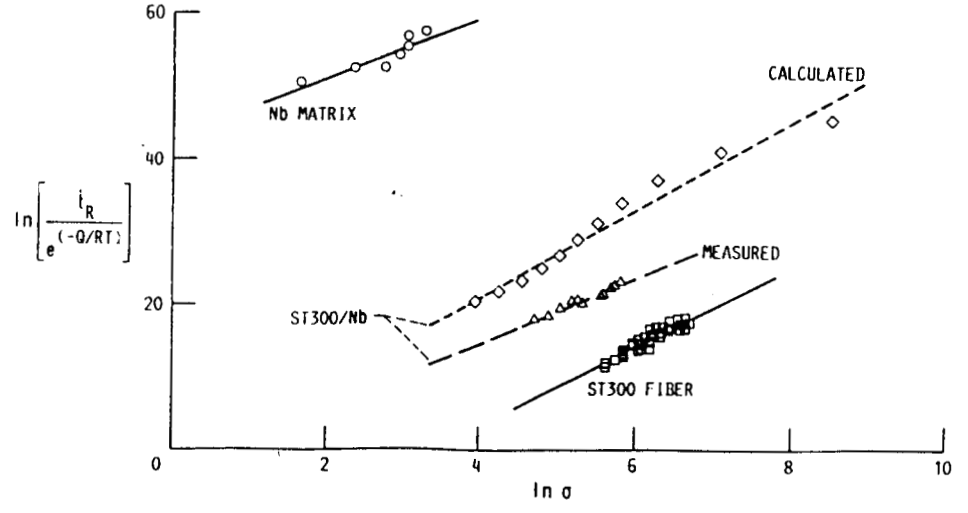

Fig 21 Comparison of matrix and fiber independent creep properties versus calculated and measured composite strengths.

thermal stresses contribute to this effect for two reasons; first, that these stresses will relax after the initial heat-up under creep conditions, and second, that the difference will tend to put more stress on the fiber and on the matrix, not less.

One effect of interdiffusion is the loss of a portion of the high-strength fiber microstructure. This effect has been shown to be minimal, however, compared to the overall strength of the composite (Figure 21).

Diffusional effects will aid in strengthening for one main reason: interdiffusion promotes a strong and ductile fiber/matrix bond. Once diffusion occurs, even to the extent that it does during fabrication, there is little chance of debonding taking place. This bond may be the most important contributor to the synergistic strengthening of the composite. By constraining the fibers and the matrix to the same amount of strain, we realize maximum strength contributions from each component in the composite. The matrix does not deform plastically even though it would without the fibers, and the fibers are kept from necking by the constraint of the rest of the fibers which are maintaining their integrity.

Effect of Matrix Alloy Additions

The effect of interdiffusion is further demonstrated if we compare the creep properties of the composites to that of the fiber itself. In Figure 22, the stress-rupture properties of ST300 fibers have been extrapolated using the Monkman-Grant (1956) relationship (which states that the time-to-rupture and the minimum creep rate are inversely proportional) to plot the theoretical time-to-1%-strain at 1500 K for a bundle of fibers assuming no surrounding matrix*. On the same graph, the time-to-1%-strain for composites with several matrix compositions is plotted.

Since the fibers contribute almost all of the composite strength, it is expected that the values for the composite and the fibers would be parallel. It is apparent from Figure 19 that, at the beginning of the test, they are comparable. As time progresses, however, the composite properties diverge negatively from the theoretical values calculated for the fibers. This can be attributed to two factors. First, the growing reaction zone removes an increasing amount of the high-strength fiber microstructure; therefore, a smaller volume fraction of fiber remains to contribute to the strength of the composite. Second, those samples

*This calculation is detailed in Appendix D.

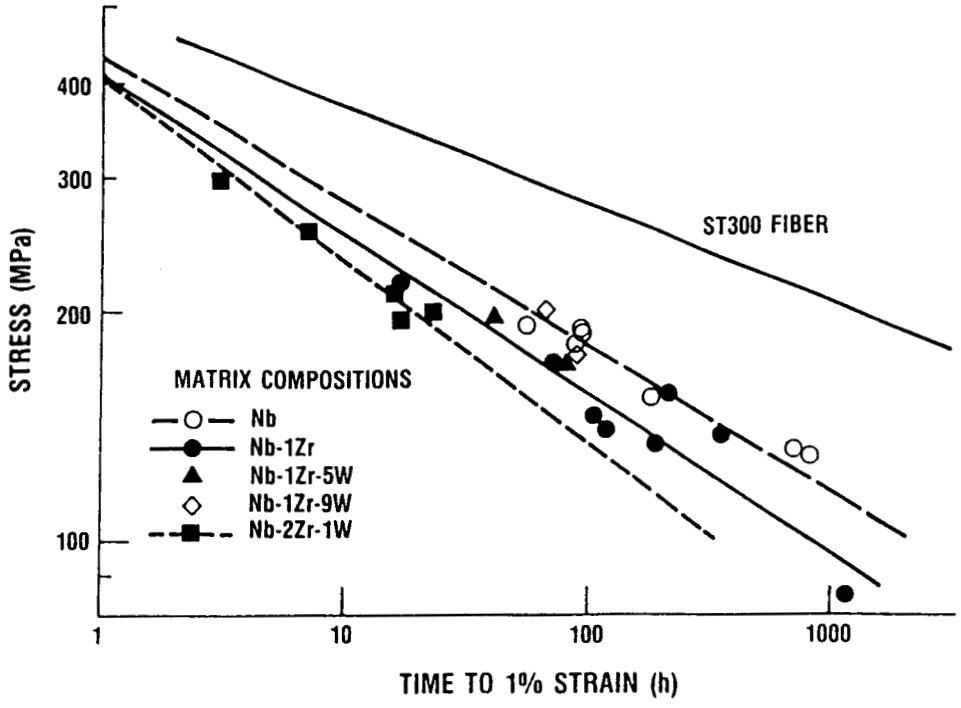

Fig 22 Comparison of the creep strength of ST300 fiber reinforced composites vs that calculated for a bundle of fibers with an equivalent cross-sectional area of fiber at 1500 K.

exposed for longer times adsorb proportionally more interstitial contaminants which may affect the strength and integrity of the matrix.

The three lines plotted for the composite properties in Figure 22 represent composites with 0, 1 and 2 w% zirconium additions to their niobium-base matrices. There is an increasing

negative deviation from the ideal fiber strength with increasing zirconium matrix content, the converse of the tensile results shown in Figure 4, where an increasing zirconium content strengthened the matrix alloys. It is possible that the addition of zirconium enhances the fiber/matrix reaction, resulting in a decrease in the volume fraction of fiber in the composite, and reducing the strength of the composite at long times. Another possibility is that the zirconia precipitate phase encourages the nucleation of Kirkendall voids at the interface; their formation is discussed in the next section.

A small number of creep data points for samples with 5 and 9 w% tungsten are also plotted in Figure 22. There is little difference in the creep strength between Nb-1Zr with and without 5 w% tungsten, whereas the addition of 9 w% tungsten appears to increase the creep resistance of the composite by ~10% at a time-to-1%-strain of 100 hr, and up to 24% at a time-to-1%-strain of 3000 hr. This may be ascribed to the higher strength of the matrix (as shown in Figure 4), to a decrease in the rate of diffusion between the tungsten fiber and the niobium alloy matrix, or a combination of the two.

These results indicate that at least 9 w% tungsten must be added to see any effect of the tungsten addition. (Therefore, the addition of less than 1 w% tungsten can be regarded as negligible.

and the decrease in strength of the Nb-2Zr-1W can be mainly attributed to the zirconium addition.) It is interesting to note that an addition of 9 w% tungsten to the matrix increases the density of a 50 v% fiber composite by approximately 3%; hence, the increase in real strength of the composite correlates to a somewhat lesser increase in its specific strength. While the addition of tungsten may impart enough additional creep resistance to the composite to make it worthwhile, longer term tests will be necessary in order to confirm and extrapolate this data.

Kirkendall Void Formation

In addition to recrystallization of the interdiffusion zone, the formation of Kirkendall voids occurs at the fiber/matrix interface. In the composite, the net mass transfer of niobium into the fiber causes a ring of very small voids to form outside of the original fiber diameter. Over time, these microvoids accumulate, and the microstructure shown in Figure 23a results. It has been noted that these voids nucleate on second phase particles, so the presence of a zirconia precipitate in the matrix may encourage their formation. These voids at the fiber/matrix interface may affect the composite properties given that the integrity of the interface area in any ductile metal-matrix composite is essential for load transfer from the matrix to the fiber. Although it is apparent from the

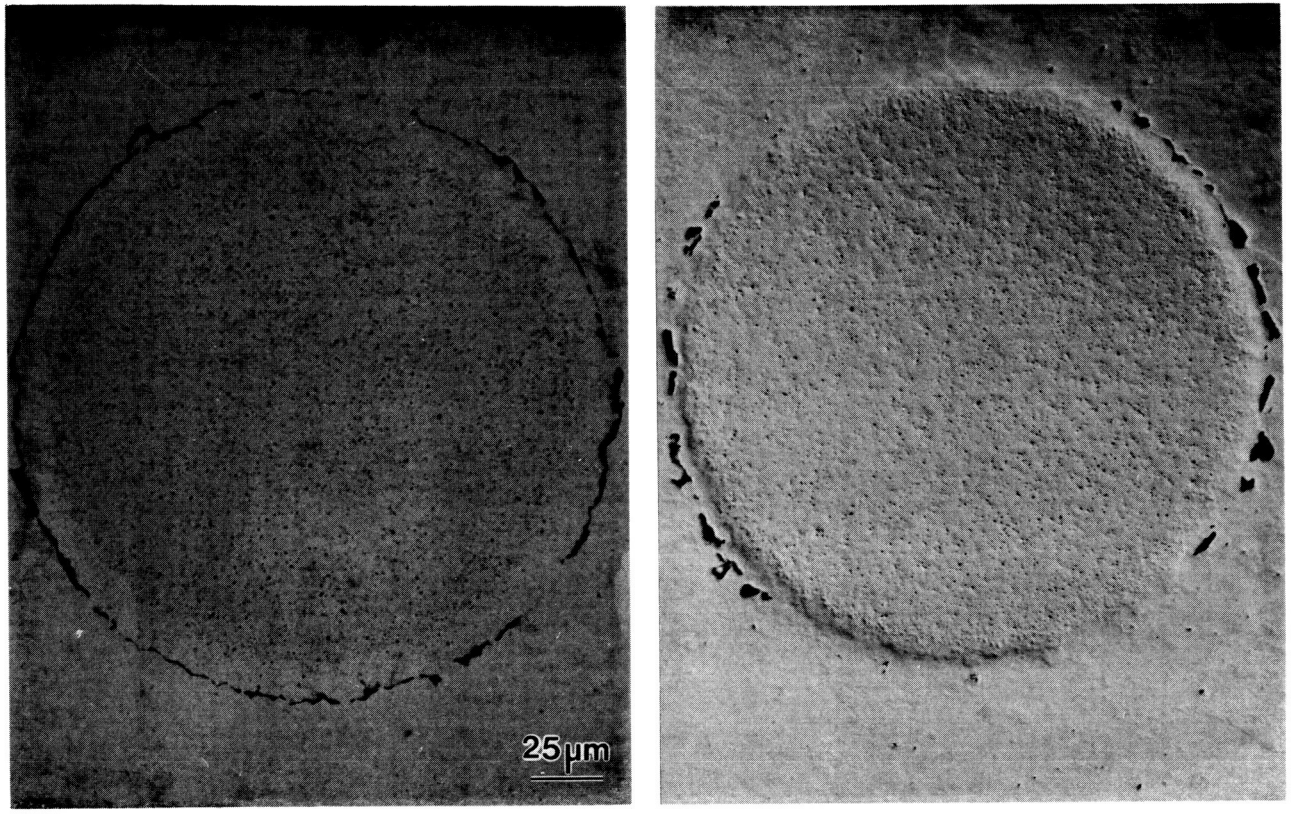

(a)

ST300/Nb
1500 K/131 MPa
2485 HR

(b)

ST300/Nb (±15^{0} ANGLE-PLIED)
1500 K/115 MPa
715 HR

Fig 23 Transverse samples in the as-polished condition reveal the presence of Kirkendall voids. The micrograph in (a) shows a single fiber in a composite panel with unidirectional axial reinforcement. The microstructure exhibits a uniform distribution of voids just outside of the original fiber diameter. The fibers in the panel in (b) were angle-plied ±15[degree] to the longitudinal axis, causing compressive stresses which suppressed the formation of voids in some areas around the fiber.

creep results that these voids do not grossly affect the axial properties of the composites, it is probable that they will have a detrimental effect on the transverse strength.

Kirkendall void formation was apparent when the fibers were angle-plied ±15°, but only on two "sides" of the fiber. This is illustrated in Figure 23b, where the long transverse direction of the composite panel is in the vertical direction in the micrograph. When the fibers are angle-plied, compressive stresses are induced on two "sides" of the fiber due to the forces which are attempting to pull the fibers parallel to the strain axis. These compressive stresses inhibit the formation of Kirkendall voids in some area around the fiber diameter (Barnes and Mazey 1958). Voids form in the remaining areas just as they do in the unidirectionally reinforced composites. Angle-plying of the fibers can therefore augment the transverse properties of the composite in two ways. First, some of the applied stress in the transverse direction is transferred to the longitudinal direction of the fibers. Second, the induced compressive stresses appear to improve the fiber/matrix bond, thereby increasing load transfer across the interface.

Micrographs of the fracture surface in composites with transversely oriented fibers (Figure 12) indicate that the failure is due to ductile deformation in the matrix rather than failure at the fiber/matrix interface or cleavage of the fiber. Furthermore, the

creep strength of the specimens with transverse fibers are slightly stronger than matrix-only samples. However, these specimens were not exposed for very long times, and the void formation may not be as developed as it would be at longer exposures. However, the applied stress on the fiber/matrix interface in the transverse oriented samples would certainly encourage void production. At longer exposures, excessive void formation at the interface may dominate failure of the composite.

Effect of Fiber Orientation

The creep strength of the composite decreases as the fiber orientation with respect to the stress axis changes (Figure 24). Conversely, the transverse properties will increase. This type of data is especially useful when designing tubing made from composite materials.

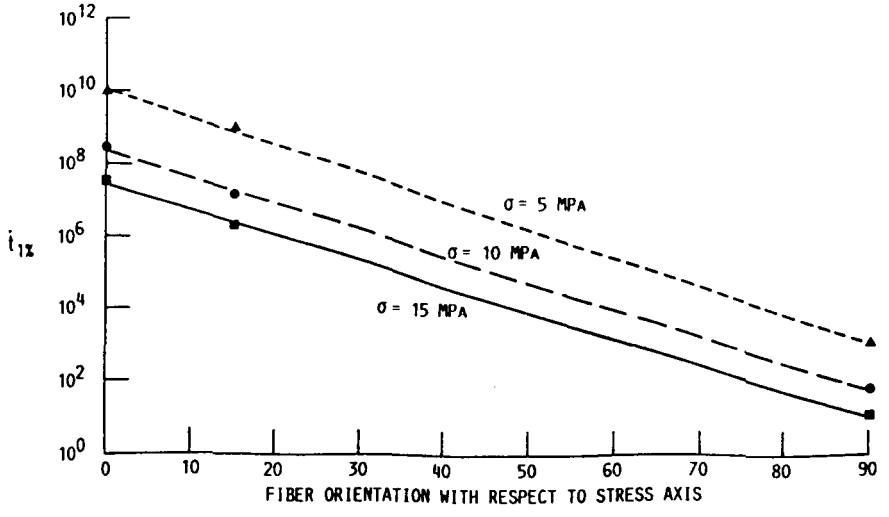

Fig 24 Effect of fiber orientation with respect to the applied stress on the creep properties of W/Nb composites.

CONCLUSIONS

Fiber Reinforcement

It has been shown that reinforcement with ST300 fibers increases the creep resistance of these niobium alloys significantly. In fact, the measured properties of the composite exceeded those calculated by the rule of mixtures. The strength properties of the individual components was apparently increased in the composite versus in stand-alone tests. This may be attributable to the constraint the fibers exert on the matrix and on each other, preventing plastic deformation. The fiber/matrix reaction, however, tends to degrade the composite creep-rupture properties at long times. Although this degradation is partially due to recrystallization of a reaction zone in the fiber, it may also be due to related Kirkendall void formation which can affect load transfer.

Fiber Orientation

The strength of composites with fibers angle-plied ±15° is decreased about 20% compared to that for composites with unidirectional, axially aligned fibers. This is apparent when comparing the time-to-rupture (Figure 13) and the minimum creep rate (Figure 14). Short term creep tests of transverse fiber reinforced composites revealed failure in the matrix, and the properties (only about 10% of the reinforced material) reflected this.

Matrix Alloying Additions

Matrix alloying additions of 9 w% tungsten appear to increase the creep resistance of W/Nb composites, although this increase is partially offset by an increase in the density of the composite. There is no indication of an effect of smaller additions of tungsten to the niobium matrix on the composite properties, but small additions of zirconium apparently cause a slight increase in the fiber/matrix interdiffusion rates, thereby lowering the creep resistance of the composite.

Comparison to Monolithic Niobium Alloys

Figure 25 compares the time-to-1%-strain of unidirectionally reinforced composites to angle-plied composites, monolithic Nb-1Zr, and monolithic PWC-11 alloy (Nb-1Zr-0.06C) at 1500 K (Titran et al, 1988). Composites with angle-plied fibers ($\pm 15^{\circ}$) are approximately 20% weaker than unidirectionally reinforced panels, but exhibit approximately the same stress exponent, indicating that the same creep mechanisms are at work. All of the composite materials are approximately an order of magnitude stronger than monolithic Nb-1Zr, and are ~4 times stronger than the PWC-11 alloy at this temperature. In addition, the creep data generated in this study can be used to predict the allowable stresses of W/Nb composite materials for a lifetime of seven years (Figure 26).

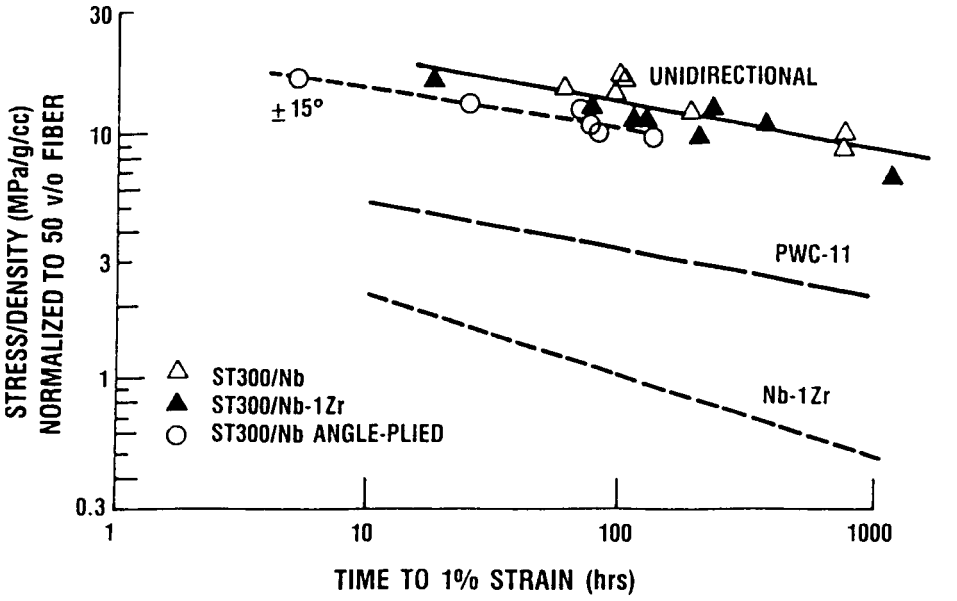

Fig 25 Comparison of the time-to-1%-strain for ST300 fiber-reinforced composites and the monolithic Nb alloys Nb-1Zr and PWC-11 (Nb-1Zr-0.06C) (after Titran et al 1988). All data is plotted on a stress-to-density basis, and the composite data was normalized to 50 v% fiber.

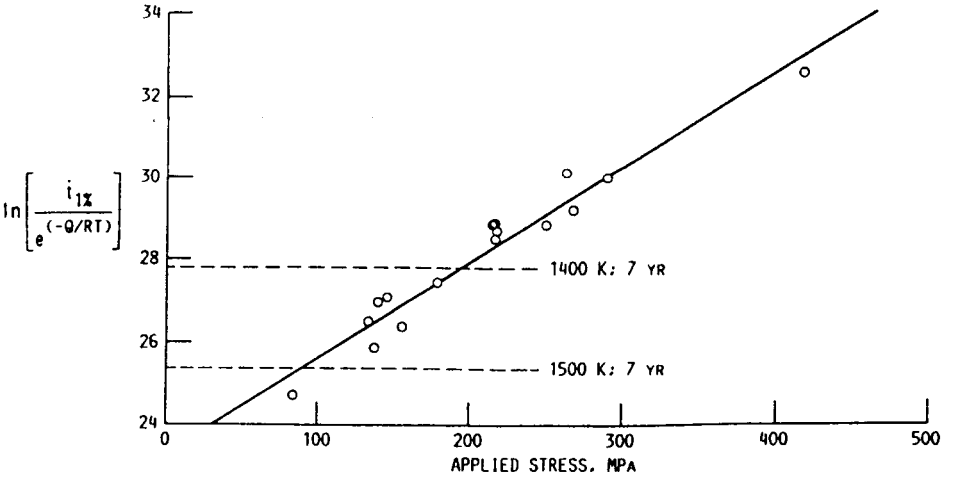

Fig 26 Orr-Sherby-Dorn plot showing the allowable stress levels to limit W/Nb composites to less than 1% strain in 60000 hours at 1400 and 1500 K.

Future Applications

Tungsten fiber reinforcement is a viable method of strengthening niobium alloys. It is apparent, however, that degradation of the creep properties of the composite occurs with long term elevated temperature exposure. Small additions of tungsten and zirconium to the matrix do not appear to affect the diffusion kinetics sufficiently to allow the use of this material for very long times (up to 7 years), although it is possible that larger additions may be more effective. This would, however, defeat the objective of not altering the chemistry of the matrix alloy significantly. It seems clear, therefore, that more direct methods of stopping or slowing the interdiffusion must be developed before this composite can be applied in a long-life application requiring creep resistance at temperatures above 1400 K.

REFERENCES

Arcella, F.G.: Interdiffusion Behavior of Tungsten or Rhenium and Group V and VI Elements and Alloys of the Periodic Table, Part 1. (WANL-M-FR-74-005-PT1, Westinghouse Astronuclear Laboratory, NASA Contract NAS3-13231) NASA CR-134490, 1974.

Barnes, R.S.; and Mazey, D.J.: The Effect of Pressure Upon Void Formation in Diffusion Couples. Acta Met., vol. 6, no. 1, Jan. 1958, pp. 1-7.

Begley, R.T.; Harrod, D.L.; and Gold, R.E.: High Temperature Creep and Fracture Behavior of the Refractory Metals. Refractory Metals Alloys, I., Machlin, R.T. Begley, and E.D., Weisert, eds., Plenum Press, New York, 1968, pp. 41-83.

Bradt, R.C.; Lenel, F.V.; and Ansell, G.S.: Kirkendall-Effect Densification in Sintered Tungsten-Molybdenum Powder Compact. Acta Met., vol. 14, No. 4, Apr. 1966, pp. 533-534.

Braint, C.T.: On the Growth of Creep Voids from Potassium-Filled Bubbles in Tungsten Wire. Scripta Met., vol. 22, no. 10, Oct. 1988, pp. 1665-1669.

Gregory, D.P.; and Rowe, G.H.: Mechanisms of Creep in Columbium and Columbium-1% Zirconium Alloy. Columbium Metallurgy, D.L. Douglass, and F.W. Kunz, eds., Interscience, New York, 1961, pp. 309-341.

Hehemann, R.F.; and Leber, S.: Chemical Diffusion in the Columbium-Tungsten System. Trans. AIME, vol. 236, 1966, pp. 1040-1044.

Hoffman, E.E.; and Harrison, R.W.: The Compatibility of Refractory Metals with Liquid Metals. Report GESP-15, General Electric Nuclear Systems Division, Cincinnati, OH, 1968.

Kopp, M.W.; and Tien, J.K.: A Preliminary Study of Ion-Implanated Diffusion Barriers in High Temperature Metal Matrix Composites. Scripta Met., vol. 22, no. 9, Sept. 1988, pp. 1527-1530.

Kopp, M.W.; Tien, J.K.; and Petrasek, D.W.: Reaction Kinetics Between Fiber and Matrix Components in Metals Matrix Composites. Superalloys 1988, S. Reichman, D.N. Duhl; G. Maurer, S. Antolovich and C. Lund, eds., TMS, Warrendale, PA, 1989, pp. 193-201.

Larson, F.R.; and Miller J.: Time-Temperature Relationship for Rupture and Creep Stresses. ASME Trans., vol. 74, no. 5, June 1952, pp. 765-775.

Lundy, T.S.; and Pawel, R.E.: Effects of Short-Circuiting Paths on Diffusion Coefficience Measurements. Trans. AIME, vol. 245, no. 2, Feb. 1969, pp. 283-286.

Lyubimov, V.D.; Gel'd, P.V; Shveykin, G.P.; and Sutina, YuA,: Self-Diffusion of Niobium in its Alloys with Tungsten. Isvestiya AN SSSR, Metally, vol. 2, 1967, pp. 84-87. (Translated in Russian Metallurgy, 1967, pp. 40-43.)

McDanels, D.L.: Analysis of Stress-Rupture and Creep Properties of Tungsten Fiber Reinforced Copper Composites. Fiber-Strengthened Metallic Composites, ASTM-STP-427, 1967, ASTM, pp. 124-148.

McDanels, D.L.; Jech, R.W.; and Weeton, J.W.: Metals Reinforced with Fibers. Met. Prog., vol. 78, no. 6, Dec. 1960, pp. 118-121.

Monkman, F.C.; and Grant, N.J.: An Empirical Relationship Between Rupture Life and Minimum Creep Rate in Creep-Rupture Tests. ASTM Proc., vol. 56, 1956, pp. 593-605.

Mundy, J.N.; Ockers, S.T.; and Smedskjaer, L.C.: Dehancement of Impurity and Self-Diffusion in Niobium by Tungsten Additions. Phys. Rev. B, vol. 33, no. 2, Jan. 15, 1986, pp. 847-853.

Orr, R.L.; Sherby, O.D.; and Dorn, J.E.: Correlations of Rupture Data for Metals at Elevated Temperatures. Trans. ASM, vol. 46, 1954, p. 113.

Petrasek, D.W.; and Signorelli, R.A.: Stress-Rupture and Tensile Properties of Refractory-Metal Wires at 2000° and 2200 °F (1093° and 1204 °C). NASA TN D-5139, 1969.

Petrasek, D.W.: High-Temperature Strength of Refractory-Metal Wires and Consideration for Composite Applications. NASA TN D-6881, 1972.

Petrasek, D.W.; and Beremand, G.: Unpublished Data. NASA Lewis Research Center, Cleveland, OH, 1987.

Petrasek, D.W.; and Titran, R.H.: Creep Behavior of Tungsten/Niobium and Tungsten/Niobium-1% Zirconium Composities. DOE/NASA/16310-5, NASA TM-100804, 1988.

Reed-Hill, R.E.: Physical Metallurgy Principles. 2nd ed., Van Nostrand, New York, 1973, pp. 378-429.

Smigelskas, A.D.; and Kirkendall, E.O.: Zinc Diffusion in Alpha Brass. Trans. AIME, vol. 1. 171, 1947, pp. 130-142.

Tietz, T.E.; and Wilson, J.W.: Behavior and Properties of Refractory Metals. Stanford University Press, Stanford, CA, 1965.

Titran, R.H.; and Hall, R.W.: High-Temperature Creep Behavior of a Columbium Alloy, FS-85. NASA TN D-2885, 1965.

Titran, R.H.; Stephens, J.R.; and Petrasek, D.W.: Refractory Metal Alloys and Composities for Space Nuclear Power Systems. DOE/NASA/16310-8 Report, NASA TM-101364.

Trefilov, V.I.; Karpinos, D.M.; Tuchinskii, L.I.; Mosieev, V.F.; Gorb, M.L.; Vishnyakov, L.R.; Pechkovskii, E.P.; Vasil'ev, A.D.; and Kokhanyi, V.A.: Plastic Deformation and Fracture of Niobium Reinforced with Tungsten Fibers. Poroshkovaya Metallurgiya, vol. 5, 1976, pp. 63-67. Translated in Soviet Powder Metallurgy and Metal Ceramics, vol. 15, no. 5, Oct. 1976, pp. 381-384.

Tuchinsky, L.I.: Thermodynamic Method of Calculating the Effect of Alloying Additives on Interphase Interaction in Composite Materials. Fizika i Khimia Obrabotka Materialov 1, 1979, pp. 121-125. Translated in Report NASA TM-88391, 1986.

Veltri, R.D.; Paradis, E.L.; and Douglas, F.C.: Investigation to Develop a Method to Apply Diffusion Barriers to High Strength Fibers. NASA CR-134719, 1975.

Welsch, G.; Young, B.J.; and Heheman, R.F.: Recovery and Recrystallization of Doped Tungsten. Strength of Metals and Alloys, Vol. V, P. Haasen, V. Gerold; and G. Kostorz, eds., Pergamon, New York, 1979, pp. 1693-1698.

Welsch, G.; Kim, K.T.; and Wang, J.J.: Potassium-Implanted Tungsten Fibers in Nickel-Base Superalloy for Study of Reaction Barrier. Final Report for NASA NAG 3-67, Case Western University, Cleveland, OH, 1987.

Westfall, L.J.: Tungsten Fiber Reinforced Superalloy Composite Monolayer Fabrication by an Arc-Spray Process. NASA TM-86917, 1985.

Westfall, L.J.; McDanels, D.L.; Petrasek, D.W.; and Grobstein, T.L.: Preliminary Feasibility Studies of Tungsten-Niobium Composites for Advanced Space Power Systems Applications. NASA TM-87248, 1986.

Ye, T.T.; Botta, W.J.; Labun, P.A.; Christian, J.W.; and Taylor, G.: Structure and Orientation of Zirconia in a Niobium Metal Matrix. Acta Met., vol. 33, 1985, pp. 477-486.

Yih, S.W.H.; and Wang, C.T.: Tungsten. Plenum Press, New York, 1979, pp. 270-299.

Appendix A. Multiple Linear Regression

The following is a sample MINITAB calculation. The columns contain the following data:

c1	Temperature (K)
c2	Normalized applied stress (MPa)
c3	time-to-1%-strain (h)
c4	1/T
c5	ln (σ)
c6	ln (.01 / $t_{1\%}$)
c7	temperature compensated time
c9	counter; in the plot "A" = 1400 K; "B" = 1500 K

MTB > print c1-c9

ROW	C1	C2	C3	C4	C5	C6	C7	C9
1	1400	216	238	0.0007143	5.37528	-10.0774	28.8168	1
2	1400	217	340	0.0007143	5.37990	-10.4341	28.4602	1
3	1400	218	277	0.0007143	5.38450	-10.2292	28.6651	1
4	1400	250	240	0.0007143	5.52146	-10.0858	28.8085	1
5	1400	263	70	0.0007143	5.57215	-8.8537	30.0406	1
6	1400	268	173	0.0007143	5.59099	-9.7585	29.1358	1
7	1400	290	79	0.0007143	5.66988	-8.9746	29.9197	1
8	1400	417	6	0.0007143	6.03309	-6.3969	32.4974	1
9	1500	84	1099	0.0006667	4.43082	-11.6073	24.6940	2
10	1500	133	190	0.0006667	4.89035	-9.8522	26.4491	2
11	1500	137	349	0.0006667	4.91998	-10.4602	25.8411	2
12	1500	139	119	0.0006667	4.93447	-9.3843	26.9170	2
13	1500	145	106	0.0006667	4.97673	-9.2686	27.0327	2
14	1500	155	212	0.0006667	5.04343	-9.9618	26.3396	2
15	1500	179	72	0.0006667	5.18739	-8.8818	27.4195	2
16	1500	217	17	0.0006667	5.37990	-7.4384	28.8630	2

*Minitab computer software, Release 5, December 1986. Minitab, Inc., 3081 Enterprise Drive, State College, PA 16801.

```
MTB > regress c6 2 c5 c4

The regression equation is
C6 = 2.92 + 4.78 C5 - 54452 C4

Predictor       Coef          Stdev      t-ratio
Constant       2.920          3.893         0.75
C5            4.7832         0.5182         9.23
C4            -54452           8209        -6.63

s = 0.4798      R-sq = 86.9%     R-sq(adj) = 84.9%

Analysis of Variance

SOURCE        DF           SS           MS
Regression     2      19.8706       9.9353
Error         13       2.9924       0.2302
Total         15      22.8630

SOURCE        DF       SEQ SS
C5             1       9.7417
C4             1      10.1289

MTB > let c7 = c6 + c4*54452
MTB > lplot c7 c5 c9
```

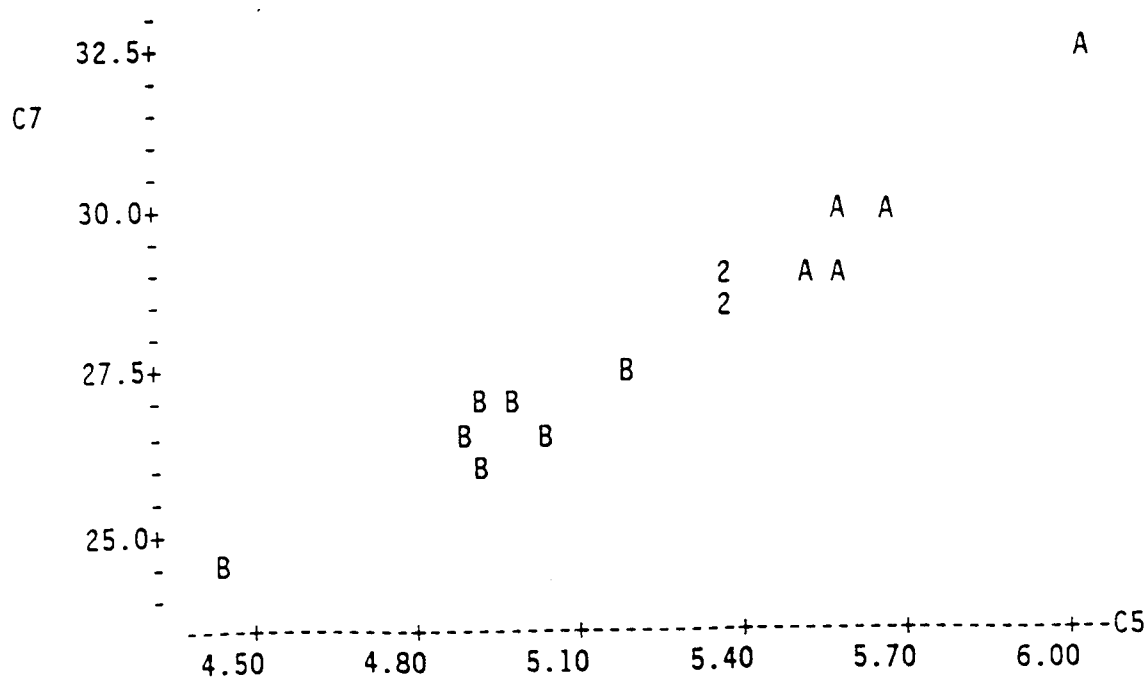

Appendix B. Volume Fraction Determination

The accepted method to determine volume fraction of a composite is to first weigh the composite structure, etch away either the matrix or fiber material, then weigh the remainder; the volume fraction can then be computed. This technique is most useful when the fibers are discontinuous or have a very small diameter. Its main disadvantage lies in measurements when there are more than two components, such as an interface layer between the fiber and matrix.

In the case of tungsten fiber reinforcement, a simpler approach is to measure the cross sectional area of the panel, count the number of fibers in that cross section, and (knowing the fiber diameter), calculate the area fraction, which equals the volume fraction. The amounts of any other phases in the composite whose area can be measured, such as a reaction zone, can be measured and taken into account in this calculation. This technique assumes two things; first, that the fibers are unbroken and extend through the length of the panel, and second, that the diameter of the fiber is relatively invariant.

Calculation of Volume Fractions

Assumptions:

We will assume that the entire affected reaction zone is inside the original fiber diameter, as shown in Figure 27. This assumption is reasonable considering the microprobe results (Figure 15) and the appearance of the recrystallized reaction zone (Figure 18). Also, since ST300 wire is a powder metallurgy product, it may contain enough porosity to accomodate the influx of mass from the matrix (Bradt et al 1966).

D_o = original fiber diameter

x = reaction zone width

D = unreacted fiber diameter (= D_o - $2x$)

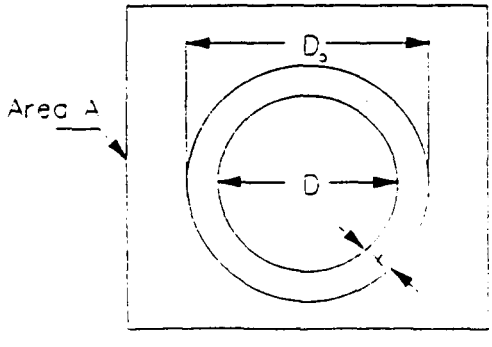

Schematic of reacted fiber in a matrix.

In addition, we assume that initially, $v_m = v_f = 0.5$, and that $v_z = 0$. If we assume a single fiber in Area A, the initial volume fraction of matrix is,

$$v_m = \frac{A - \frac{\pi D_o^2}{4}}{A} = 1 - \frac{\pi D_o^2}{4A} = .5$$

This expression equals 0.5 since the volume fraction of the matrix remains constant. This can be solved to find an expression for A,

$$A = \frac{\pi D_o^2}{2}$$

The volume fraction of fiber is equal to,

$$v_f = \frac{\pi D^2}{4A} = \frac{\pi}{4A}(D_o - 2x)^2 = \frac{(D_o - 2x)^2}{2D_o^2}$$

and the volume fraction of the interface zone is,

$$v_z = \frac{\frac{\pi D_o^2}{4} - \frac{\pi D^2}{4}}{A} = \frac{\frac{\pi}{4}(D_o^2 - D^2)}{\frac{\pi D_o^2}{2}} = 0.5 - \frac{(D_o - 2x)^2}{2D_o^2}$$

Appendix C. Rule of Mixtures Calculation

```
'This program calculates the creep strength of a W/Nb composite using'
'the rule of mixtures.  The creep strength of the fiber and matrix are'
'measured, and the creep strength of the reaction zone is varied'
'between that of the fiber and the matrix by the variable R'

  for R = 0 to 1. step .5

'Cycle temperature to generate data points'
  for T  = 1000 to 2000 step 100        'T is temperature in K'

'Set constants'
  let D  = 200            'D is original fiber diameter'
  let tm = 100            'tm is time in hours'

'Calculate the width of the reaction zone'
  let A  = exp (-0.5 * (37390/T + 3.869))
  let x  = A * tm^0.5 * 6 * 10^5

'Calculate the volume fractions of matrix, fiber, and zone'
  let vm = .5
  let vf = ((D - 2*x)^2)/(2*D^2)
  let vz = ((D^2 - ((D - 2*x)^2)))/(2*D^2)

'Calculate creep strength of matrix and fiber'
  let sm = (1/tm)^.24 * 3.4 * 10^(-5) * exp (20384/T)
  let sf = (1/tm)^.152 * 48.2 * exp (4153/T)

'Estimate the creep strength of the reaction zone'
'If R=0, sz = sm; if R=1, sz = sf'
  let sz = sf * R + sm * (1.-R)

'Calculate the creep strength of the composite'
  let sc = sm * vm + sf * vf + sz * vz

  let y  = 50000/T - log(tm)
  let x  = log(sc)

  print T,tm,R,y,x

  next T
  next R
```

temp	time	ratio	y	x
1000	100	0	45.39483	8.470425
1100	100	0	40.84937	7.048043
1200	100	0	37.0615	6.24327
1300	100	0	33.85637	5.786394
1400	100	0	31.10912	5.473395
1500	100	0	28.72816	5.209218
1600	100	0	26.64483	4.941931
1700	100	0	24.80659	4.622714
1800	100	0	23.17261	4.177294
1900	100	0	21.71062	3.441844
2000	100	0	20.39483	1.78867
1000	100	0.5	45.39483	8.47038
1100	100	0.5	40.84937	7.04801
1200	100	0.5	37.0615	6.243983
1300	100	0.5	33.85637	5.790243
1400	100	0.5	31.10912	5.485968
1500	100	0.5	28.72816	5.242216
1600	100	0.5	26.64483	5.018569
1700	100	0.5	24.80659	4.789115
1800	100	0.5	23.17261	4.532011
1900	100	0.5	21.71062	4.234017
2000	100	0.5	20.39483	3.927832
1000	100	1	45.39483	8.470335
1100	100	1	40.84937	7.047977
1200	100	1	37.0615	6.244695
1300	100	1	33.85637	5.794077
1400	100	1	31.10912	5.498384
1500	100	1	28.72816	5.274159
1600	100	1	26.64483	5.089749
1700	100	1	24.80659	4.931736
1800	100	1	23.17261	4.793318
1900	100	1	21.71062	4.670425
2000	100	1	20.39483	4.560298

Appendix D. Extrapolation of Fiber Stress-Rupture Data

The equation for the minimum creep rate line on a typical creep curve is

$$y = mx + b \quad \text{or} \quad 1 = (mcr)(t_{1\%}) - b.$$

In addition, it has been determined from the experimental creep curves for ST300/Nb and ST300/Nb-1Zr (values in Table X) that $b \approx 0.292$. Therefore,

$$(mcr)(t_{1\%}) = 1 - 0.292 = 0.708.$$

In addition, Monkman and Grant (1956) found that,

$$(mcr)(t_R) = 0.036$$

$$\therefore \quad \frac{0.708}{t_{1\%}} = \frac{0.036}{t_R}$$

$$t_R = \left(\frac{0.036}{0.708}\right) \cdot t_{1\%} = (0.051) \cdot t_{1\%}.$$

In addition, the approximate relationship between the time-to-rupture, applied stress, and temperature for the ST300 fibers was found to be (Eqn 7),

$$t_R = (8.42 \times 10^{-12}) \sigma^{6.58} e^{-\frac{27000}{T}}$$

$$\therefore \quad \frac{1}{t_{1\%}} = (1.28\times 10^{-19})\sigma^{6.58} = \frac{1}{(0.051)t_{1\%}}$$

$$\therefore \quad t_{1\%} = \frac{1}{(0.051)(1.28\times 10^{-19})\sigma^{6.58}} = \frac{1.53\times 10^{20}}{\sigma^{6.58}}$$

$$\therefore \quad \sigma = \frac{1168}{(t_{1\%})^{.152}}$$

We now have an approximate relationship between the normalized applied stress and the time-to-1%-strain for the ST300 fibers at 1500 K.

NASA
National Aeronautics and Space Administration

Report Documentation Page

1. Report No.	2. Government Accession No.	3. Recipient's Catalog No.
NASA TM-102122 DOE/NASA/16310-10		

4. Title and Subtitle	5. Report Date
The Interface in Tungsten Fiber Reinforced Niobium Metal-Matrix Composites	September 1989
	6. Performing Organization Code

7. Author(s)	8. Performing Organization Report No.
Toni L. Grobstein	E-4754
	10. Work Unit No. 586-01-11

9. Performing Organization Name and Address	11. Contract or Grant No.
National Aeronautics and Space Administration Lewis Research Center Cleveland, Ohio 44135-3191	
	13. Type of Report and Period Covered Technical Memorandum

12. Sponsoring Agency Name and Address	14. Sponsoring Agency Code
National Aeronautics and Space Administration Washington, D.C. 20546-0001	

15. Supplementary Notes

Final Report. Prepared under Interagency Agreement DE-AI03-86SF16310. This report was submitted by Toni L. Grobstein as a thesis in partial fulfillment of the requirements for the degree Doctor of Philosophy to Case Western Reserve University, Cleveland, Ohio.

16. Abstract

The creep resistance of tungsten fiber reinforced niobium metal-matrix composites was evaluated. The interface region between the fiber and matrix was characterized by microhardness and electron probe microanalysis measurements which indicated that its properties were between those of fiber and matrix. However, the measured properties of the composite exceeded those calculated by the rule of mixtures even when the interface zone was assumed to retain all the strength of the fiber. The composite structure appeared to enhance the strengths of both the fibers and the matrix above what they exhibited in stand-alone tests. The effect of fiber orientation and matrix alloy composition on the fiber/matrix interface were also evaluated. Small alloying additions of zirconium and tungsten to the niobium matrix affected the creep resistance of the composites only slightly. A decrease in the creep resistance of the composite with increasing zirconium content in the matrix was ascribed to an increase in the diffusion rate of the fiber/matrix interdiffusion reaction, and a slight increase in the creep resistance of the composite was observed with an addition of 9 w% tungsten to the matrix. In addition, Kirkendall void formation was observed at the fiber/matrix interface; the void distribution differed depending on the fiber orientation relative to the stress axis.

17. Key Words (Suggested by Author(s))	18. Distribution Statement
Interdiffusion; Creep; Matrix-alloy effects; Fiber orientation; Angle ply; Refractory metals	Unclassified – Unlimited Subject Category 26 DOE Category UC-25

19. Security Classif. (of this report)	20. Security Classif. (of this page)	21. No of pages	22. Price*
Unclassified	Unclassified	76	A03

*For sale by the National Technical Information Service, Springfield, Virginia 22161